Available online at www.sciencedirect.com
SCIENCE DIRECT®
Coordination Chemistry Reviews 238–239 (2003) 187–209
COORDINATION CHEMISTRY REVIEWS
www.elsevier.com/locate/ccr

DFT calculations of molecular magnetic properties of coordination compounds

Ilaria Ciofini, Claude A. Daul *

Département de Chimie, Université de Fribourg, Pérolles, CH 1700 Fribourg, Switzerland

Received 22 February 2002; accepted 2 December 2002

Contents

Abstract

An overview of density functional theory (DFT) based techniques for the calculation of the magnetic properties of molecular and supramolecular assemblies is presented. Three different approaches to compute the exchange coupling constant (J^{ex}) are reviewed, i.e. the broken symmetry (BS) technique, the single determinant (SD) approach, and the spin projection method. The first one (BS), developed by Noodleman, is undoubtedly most commonly applied, e.g. to clusters containing several paramagnetic metal centres or to paramagnetic organic radical species. The second approach (SD) was originally developed to compute the electronic spectra of transition metal complexes, but was more recently applied to the computation of spin manifold of molecular magnets. The last method, developed by Ovchinnikov and Labanowsky, is mainly an extension of the Hartree–Fock (HF) concept of spin decontamination to DFT. The performance of the three methods has been evaluated for model systems (HHeH, $[Cu_2Cl_6]^{2-}$) and for more complex molecules ($Ti(CatNSQ)_2$ and $Sn(CatNSQ)_2$, Bis-verdazyl diradical (BVD), $[Fe_2(OH)_3(tmtacn)_2]^{2+}$ and $[[Cu_3O_2L_3]^{3+}$, L = *N*-Permethylated (1*R*,2*R*)-cyclohexanediamine). A comparison of these results with experimental values and with post-HF results if available is presented as well. In the case of the last two complexes, i.e. mixed valence systems, computation of the vibronic

* Corresponding author.
E-mail address: claude.daul@unifr.ch (C.A. Daul).

doi:10.1016/S0010-8545(02)00330-2

potential energy surfaces is also briefly discussed.

Keywords: DFT calculations; Molecular magnetic properties; Coordination compounds

1. Introduction

Although the magnetic behaviour of some materials, e.g. lodestone, has been well known since antiquity, a deeper understanding of the microscopic processes related to magnetic interaction is still an interesting topic in modern theoretical chemistry and a difficult task in computational chemistry [1]. The basis of the theory of magnetic interactions between paramagnetic sites was developed in the first half of this century, but even now the computational effort needed is still not generally affordable. From a theoretical point of view, scientists interested in explaining the magnetic behaviour of insulators were the first to study magnetic interactions. Two names must certainly be mentioned in this field i.e. those of J.H. Van Vleck and of P.W. Anderson who can be considered as the founders of modern magnetism.

In this contribution we borrow the definition of the late Olivier Kahn[1]: 'Molecular Magnetism deals with magnetic properties of isolated molecules and/or assemblies of molecules' to give a more pragmatic picture of the topic.

The main reason to deal with a molecular magnet instead of with common inorganic magnets e.g. of transition metals oxides is the possibility to add various other properties to the compounds such as, e.g. optical properties. The possibility to increase the complexity of the 3D architecture and exchange pathway using paramagnetic organic ligands [2] and paramagnetic metal centres [3] was an idea for several preparative approaches. On the other hand, the study of biological processes involving active sites containing metal ions is related to the interaction between paramagnetic metal centres, which is not so different from that which happens in a magnetic material [4]. This chapter will be organised as follows: after a short description of the phenomenological Spin Hamiltonian approach used to describe magnetic interactions, the unavoidable link between the interpretation of experimental data and theory, we will present in their original formulation three formalisms that have been used in the framework of DFT in order to study exchange interaction in organic and organometallic systems. Finally, an overview of the performance of the methods in the case of model and chemical systems will be given.

[1] O. Kahn, in: Molecular Magnetism, VCH publishers, 1993, p. VI.

2. Theory and computational tools

2.1. The spin Hamiltonian: a phenomenological approach

The main idea of Spin Hamiltonians is to represent the physics of the interactions between magnetic centres through spin operators which act only on local effective spin eigenfunctions. The system is therefore described through its spin eigen-states. The spin eigenfunction reads:

$$\{|S_1 S_2 S_3 \dots S_i \dots \mathrm{SM}\rangle\}$$

where, S is the total spin state due to the coupling of all the S_i's (i.e. the local spin of the i-th site).

This idea is justified in considering that e.g. for insulators the spin and the magnetic moments whose alignments lead to magnetic effects are certainly localisable, so that from a phenomenological point of view at least, their interactions can be described by spin operators acting on local spin states.

The spin Hamiltonian is not able to give electronic information on the interactions between the metal centres. But it can be used, and commonly is used, to interpret the variations of the different total spin state energies as a function of empirical parameters derived from different kind of experiments such as EPR, NMR, Mössbauer, optical spectroscopy and/or magnetic susceptibility measurements at different temperatures.

The most-commonly used Spin-Hamiltonian is the so-called HDVV [5] (Heisenberg–Dirac–Van–Vleck), which implies an isotropic interaction between the paramagnetic centres described through an exchange coupling constant J^{ex}. It is a pair interaction and amongst the different formulation found in literature[2], we will use the following notation:

$$H_{\mathrm{HDVV}} = \sum_{i>j} J_{ij}^{\mathrm{ex}} \hat{\mathbf{S}}_{\mathbf{i}} \cdot \hat{\mathbf{S}}_{\mathbf{j}} \tag{1}$$

where, **i** and **j** denote the paramagnetic centres.

In case of a dimer, the Hamiltonian can be expressed in a simpler form as:

$$H_{\mathrm{HDVV}} = J_{\mathrm{AB}}^{\mathrm{ex}} \hat{\mathbf{S}}_{\mathbf{A}} \cdot \hat{\mathbf{S}}_{\mathbf{B}} = \frac{J_{\mathrm{AB}}^{\mathrm{ex}}}{2} (\mathbf{S}^2 - \hat{\mathbf{S}}_{\mathbf{A}}^2 - \hat{\mathbf{S}}_{\mathbf{B}}^2) \tag{2}$$

If an external field is absent, each of the total spin states are $(2S+1)$-fold degenerate. Sometimes the

[2] Other notations commonly used are: $H_{\mathrm{HDVV}} = -\Sigma_{i>j} J_{ij}^{\mathrm{ex}} \hat{\mathbf{S}}_{\mathbf{i}} \cdot \hat{\mathbf{S}}_{\mathbf{j}}$; $H_{\mathrm{HDVV}} = -2\Sigma_{i>j} J_{ij}^{\mathrm{ex}} \hat{\mathbf{S}}_{\mathbf{i}} \cdot \hat{\mathbf{S}}_{\mathbf{j}}$.

HDVV spin Hamiltonian is not sufficient to describe the magnetic interaction in materials, therefore either single centres or interaction terms are added. The zero field splitting (ZFS) and the biquadratic HDVV terms are, respectively, an example of both corrections. The ZFS justify for instance the lack of degeneracy of the different M_s values for a given S total spin state in absence of external field due to the spin–orbit interaction, while the biquadratic HDVV is sometimes used to describe non-linear interaction between the magnetic centres.

A deeper description and the list of Spin Hamiltonians commonly used to interpret magnetic data can be found, for instance, in reference [6–8]. These non-Heisenberg terms are often considered as a first order perturbation to the energy obtained using a HDVV, spin-only, Hamiltonian.

As mentioned previously the use of a HDVV spin Hamiltonian presupposes that spins are localised on each centre. This phenomenon is usually called valence trapping and this description is inadequate for systems where the valence electrons can be delocalised. It is the case for mixed valence systems, where metal centres with different oxidation states are present. Anderson and Hasegawa [9] developed a spin Hamiltonian that describes these phenomena of electron delocalisation at the beginning of the 1950s and introduced the concept of double-exchange. This term may appear rather obscure to many chemists and we propose to use the term: spin dependent electron delocalisation [10] because just so-called Hound-states, i.e. states with the same spin multiplicity, will be consider to contribute to the delocalisation phenomena, as depicted in Fig. 1 below.

Later on, more complicated interactions schemes were developed, e.g. the exchange-transfer [11] model, where the delocalisation involves three centres and which can take place via non-Hound states (cf. Fig. 2).

When electron delocalisation can occur, the whole set of spin states representing the system will be:

$$\{|S_1 \ldots S_i \ldots S_n \mathrm{SM}\rangle\}_1 \otimes \ldots\ldots \{|S_1 \ldots S_i \ldots S_n \mathrm{SM}\rangle\}_i \ldots\ldots \otimes \{|S_1 \ldots S_i \ldots S_n \mathrm{SM}\rangle\}_n$$

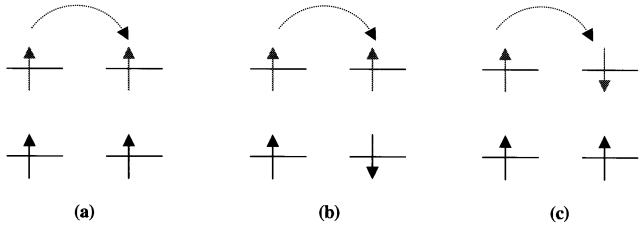

Fig. 1. Hund (a and b, without spin flip) and non-Hund (c, with spin-flip) mechanism of delocalisation.

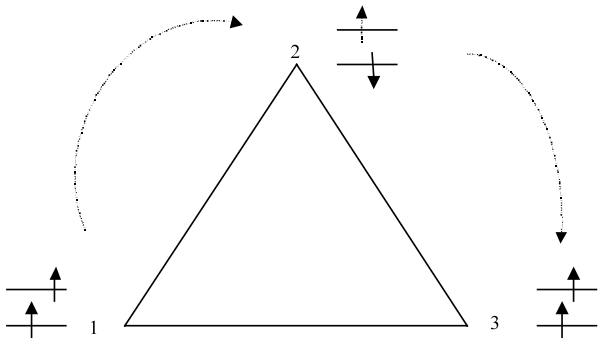

Fig. 2. Exchange transfer model.

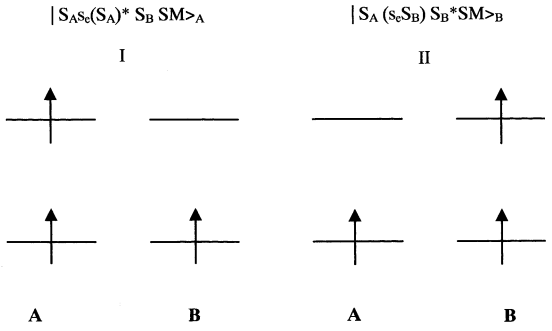

Fig. 3. Graphical representation of localised spin states for a AB dimer.

where, the subscript i indicates the centre where spin excess is localised.

To illustrate this, let us consider for the sake of clarity a dimer A–B where $S_A = 1/2 = S_B$ with a spin excess $s_e = 1/2$. Two different sets of spin states will arise, corresponding to the two different localised situations depicted in Fig. 3.

Next we define a transfer operator as:

$$H_{AB} = \beta T_{AB} \tag{3}$$

where, T_{AB} is the operator which transfer an electron from the site A to B, i.e.:

$$T_{AB}|S_A \ldots \mathrm{SM}\rangle_A = K_{AB}|S_A \ldots \mathrm{SM}\rangle_B \tag{4}$$

The resulting Hamiltonian matrix is then:

$$\begin{array}{cc} |S_A \ldots \mathrm{SM}\rangle_A & |S_A \ldots \mathrm{SM}\rangle_B \\ \begin{vmatrix} J^{ex}\hat{\mathbf{S}}_A\hat{\mathbf{s}}_e + J^{ex}(\hat{\mathbf{S}}_A + \hat{\mathbf{s}}_e)\hat{\mathbf{S}}_B & \beta \cdot \mathbf{1} \\ \beta \cdot \mathbf{1} & J^{ex'}\hat{\mathbf{S}}_B\hat{\mathbf{s}}_e + J^{ex}\hat{\mathbf{S}}_A(\hat{\mathbf{S}}_B + \hat{\mathbf{s}}_e) \end{vmatrix} \end{array} \tag{5}$$

where $J^{ex\prime}$ is the intra-atomic exchange coupling constant and J^{ex} is the inter-atomic one.

If we ignore non-Hound states we obtain:

$$\begin{vmatrix} E_A + J^{ex}\hat{\mathbf{S}}_A^*\hat{\mathbf{S}}_B & \beta \cdot \mathbf{1} \\ \beta \cdot \mathbf{1} & E_B + J^{ex}\hat{\mathbf{S}}_A\hat{\mathbf{S}}_B^* \end{vmatrix} \tag{6}$$

where, E_A and E_B are the energies of the two isolated centres when the electrons' excess is localised onto them.

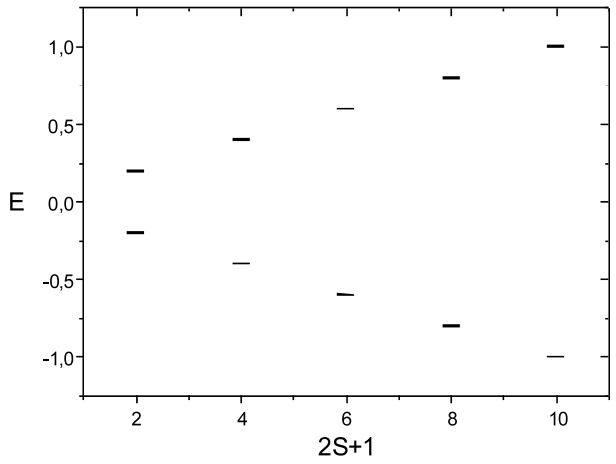

Fig. 4. Energy of the spin states (in units of β) for a d^5–d^6.

For a binuclear system i.e. one where each of the two centres has n electrons occupying the d-orbitals and a 'delocalised' electron oscillating between them ($s_e = 1/2$), Anderson and Hasegawa [9] derived the following analytical formula to express the energies of each spin state as a function of what they call the double-exchange parameter β:

$$E(S) = \pm\beta \frac{S + 1/2}{2S_0 + 1} \tag{7}$$

Due to the double exchange interaction each spin states is split into two levels corresponding to an in-phase (gerade) and an out of phase (ungerade) combination. Since the stabilisation is proportional to $S+1/2$ (in case of a dimer), it is straightforward to see that the double exchange process will favour the stabilisation of the spin state with highest multiplicity $S = S_{max}$ (cf. Fig. 4).

Finally, in the case of a mixed valence dimer, when taking into account both exchange and double exchange interactions, the energy expression of each spin state as a function of exchange (J^{ex}) and double exchange (B) parameters thus reads:

$$E(S) = \frac{J}{2}\ S(S+1) \pm B(S+1/2) \tag{7a}$$

2.2. Molecular magnetism and computational chemistry

It is well known that magnetic interactions arise from weak bonding while a strong interaction between paramagnetic centres leads to a covalent bond formation and therefore to diamagnetic molecules. It is important to find computational techniques, which are able to correctly describe these weak interactions.

A semi-quantitative evaluation of magnetic interactions and the corresponding parameters is possible using Orbital Interaction Models where a simplified Hamiltonian and limited basis-sets are used. A quantitative estimation will need the use of extensive post-HF or DFT calculations in order to fully include the dynamical and the quasi-degeneracy correlation of the electrons.

2.2.1. Semi-empirical and qualitative models

Several orbital interaction models have been developed in the seventies to describe the magnetic interaction. Amongst these, let us mention both, the model of Hoffman et al. [12] and the model of Kahn et al. [13]. Both of them have been widely used.

We will illustrate shortly the two methods next. Consider a full electronic Hamiltonian:

$$H = \sum_i h(i) + \sum_{j>i} \frac{1}{r_{ij}} + \hat{h}_{SO}$$

The following approximations are usually made:

- Active electron approximation: just the unpaired electrons are taken into account. All the inner electrons are just considered as belonging to non-interacting cores.
- The spin–orbit interaction is usually neglected.
- A minimal basis set is used
- Usually, semi-empirical methods are used to evaluate the integrals e.g. Extended Hückel (EH).

The first approximation is valid only if the magnetic orbitals, i.e. those containing the unpaired electrons, are well separated in energy, both, from the doubly occupied and from the unoccupied or virtual ones. This is not always the case.

For the sake of simplicity, only the model of Hoffman et al. [12], which is based on m. o. theory (Kahn and Briat's model is based on valence bond theory) and is usually applied within the EH formalism, will be described in some details here.

Suppose we have a dimer A–B where each of the moieties contains an unpaired electrons occupying a d-orbital. We will denote by d_A and d_B the two magnetic orbitals on site A and B, respectively. Hence, ϕ_1 and ϕ_2 will be the molecular orbitals arising from their interaction i.e.

$$\phi_1 = \frac{1}{\sqrt{2}}(d_A + d_B)$$

$$\phi_2 = \frac{1}{\sqrt{2}}(d_A - d_B) \tag{8}$$

In the absence of a strong direct interaction ($\langle d_A | d_B \rangle \approx 0$), these two orbitals will not be much perturbed.

Within the active electron approximation described here, just the configuration arising from different

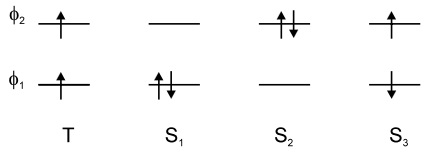

Fig. 5. Different configuration arising from the magnetic orbitals.

occupation of magnetic orbitals will be considered. Thus, we get the following spin-states: 1, triplet and 3, singlets. They are depicted below in Fig. 5 where:

$$T = |\phi_1\alpha\phi_2\alpha|; \quad S_1 = |\phi_1\alpha\phi_1\beta|; \quad S_2 = |\phi_2\alpha\phi_2\beta|;$$

$$S_3 = \frac{1}{\sqrt{2}}(|\phi_1\alpha\phi_2\beta| - |\phi_1\beta\phi_2\alpha|)$$

Within this manyfold, the triplet state is unique, and does therefore, not interact if spin–orbit coupling is neglected. The singlet states however do and can be expressed as:

$$\psi_S = \lambda_1\psi_{S_1} + \lambda_2\psi_{S_2} + \lambda_3\psi_{S_3} \tag{9}$$

Usually $\lambda_3 \approx 0$ since ϕ_1 and ϕ_2 often belong to two different, or almost different, irreducible representations. Thus, ψ_{S_3} has a different symmetry than ψ_{S_2} and ψ_{S_1}, and does therefore, not interact.

The triplet state is correctly described by the single determinant (SD) ψ_T. In the case of non-interacting orbitals (ϕ_1 and ϕ_2 are degenerate): $\lambda_1 = \lambda_2$. While for an interacting system, we have $|\lambda_1| \gg |\lambda_2|$.

At this level of approximation, the energies of the states can be expressed in terms of Coulomb (J_{12}), Exchange (K_{12}) and core matrix elements (h_i). Thus:

$$E_{\text{Tripl.}} - E_{\text{Sing.}} = J_{12} - K_{12} - \frac{1}{2}(J_{11} + J_{22}) + \frac{1}{2} \times [(2h_1 + J_{11} - 2h_2 + J_{22})^2 + 4K_{12}^2]^{1/2} \tag{10}$$

where:

$$h_i = \langle\phi_i(1)|h(1)|\phi_i(1)\rangle;$$

$$J_{12} = \left\langle \phi_1(1)\phi_2(2)\left|\frac{1}{r_{12}}\right|\phi_1(1)\phi_2(2)\right\rangle;$$

$$K_{12} = \left\langle \phi_1(1)\phi_2(2)\left|\frac{1}{r_{12}}\right|\phi_1(2)\phi_2(1)\right\rangle$$

This can be rewritten in terms of orthogonal and localised orbitals ϕ_A and ϕ_B mainly centred on site A and B i.e.

$$\phi_A = \frac{1}{\sqrt{2}}(\phi_1 + \phi_2)$$

$$\phi_B = \frac{1}{\sqrt{2}}(\phi_1 - \phi_2) \tag{11}$$

Thus, the singlet to triplet energy difference can be evaluated as:

$$E_{\text{Tripl.}} - E_{\text{Sing.}} = -2K_{AB} + \frac{(\varepsilon_1 - \varepsilon_2)^2}{J_{AA} - J_{AB}} \tag{12}$$

where $\varepsilon_1 = h_1 + J_{12} - K_{12}$ and $\varepsilon_2 = h_2 + J_{12} - K_{12}$.

Moreover, since:

$$\varepsilon_1 - \varepsilon_2 = h_1 - h_2\langle\phi_1 + \phi_2|h|\phi_1 - \phi_2\rangle = 2h_{AB}$$

we get the final expression:

$$E_{\text{Tripl.}} - E_{\text{Sing.}} = 2K_{AB} + \frac{(2h_{AB})^2}{J_{AA} - J_{AB}} = J_{AB}^{ex} \tag{13}$$

From these expressions we can derive some qualitative conclusions regarding the stabilisation of a ferromagnetic (triplet) versus an anti-ferromagnetic (singlet) ground state. It is evident that two antagonistic contributions to the exchange-coupling constant (J_{AB}^{ex}) do exist: (i) a ferromagnetic one: J_F and (ii) an anti-ferromagnetic one: J_{AF}.

Considering that the exchange integral K_{AB} is always positive, the contribution:

$$J_F = -2K_{AB}$$

will favour the ferromagnetic interaction (the triplet is the ground state). This term is referred to as 'potential exchange' in Anderson's theory [14].

The second contribution:

$$J_{AF} = \frac{(2h_{AB})^2}{J_{AA} - J_{AB}}$$

will on the other hand favour the anti-ferromagnetic interaction. The term J_{AB} is usually referred to as 'kinetic exchange' [14].

This model can be extended to any binuclear system containing m electrons per site. The general expression is:

$$J^{ex} = J_F + J_{AF} \tag{14}$$

where

$$J_F = -\frac{2}{m^2}\sum_{i\in A}\sum_{j\in B} K_{ij} \tag{15}$$

$$J_{AF} = \frac{1}{m^2}\sum_{i=1}^{m}\frac{(\varepsilon_{2i} - \varepsilon_{2i-1})^2}{J_{Ai,Ai} - J_{Ai,Bi}} \tag{16}$$

Before passing to non-empirical techniques, it is worthwhile to mention a fully empirical approach developed in the 1950s which is based on the overlap between the two magnetic orbital and which does remarkably well predict the ferro- or anti-ferromagnetic nature of their interaction. We summarize below briefly the so-called Goodenough–Kanamori [15] rules:

- When the interacting centres have the lobes of the magnetic orbitals directly pointing towards each others and when the overlap between them is substantial, then the interaction (direct exchange) is strongly anti-ferromagnetic.
- If a magnetic orbital of one centre overlaps with an empty orbital of the other centres the direct interaction is ferromagnetic.
- When the magnetic orbitals are orthogonal and hence the overlap is zero, then the direct interaction is ferromagnetic.

The interaction can occur also through diamagnetic ligands, which have doubly occupied or empty orbitals. In this case the interaction is referred to as super-exchange.

A classic example of failure of the semi-empirical models mentioned before is given by the study of the magnetic behaviour of one of the first molecular magnetic material synthesised, i.e. the diaquo-tetra-μ-acetato-dicopper(II). In this case, the two copper(II) are antiferromagnetically coupled and the separation between the lowest singlet and the lowest triplet has been estimated from magnetic susceptibility data as equal to 296 cm^{-1} [16].

In Fig. 6 we reported the singlet–triplet energies separation computed [17] at different levels of theory and compared with the experimental one.

It is easy to notice that we need a post Hartree–Fock (HF) treatment in order to obtain a quantitative agreement with the experimental J-value. Moreover, the simple Anderson approach is completely wrong! Why?

In fact, the reason is simple in this case. The main approximation (active electron) is not correct and several configurations are to be taken into account in order to reproduce the data correctly.

Generally speaking, we need a computational tool, which is able to include correlation and to reproduce the intrinsic multi-determinantal nature of the spin manifolds.

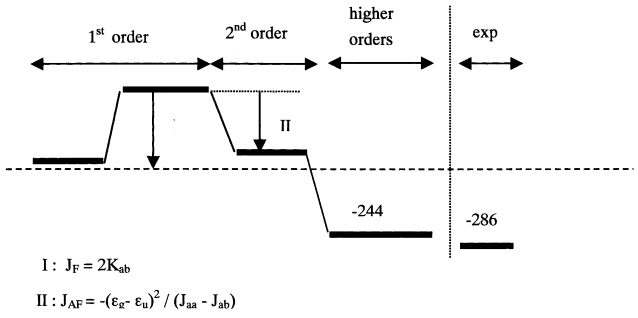

Fig. 6. Computed singlet–triplet separation (in cm^{-1}) for diaquate-tra-μ-acetato-dicopper(II). Where the ferromagnetic contribution (eq. (15)) and the antiferromagnetic one (eq. (16)) are denoted first and second order, respectively.

Post-HF techniques are certainly good candidates. Unfortunately, they can only be used for relatively small systems. As soon as the dimension of the system increases, the consideration of extended configuration interactions to account for correlation and of huge basis sets needed to represent correctly the electron cusp, render these approaches frequently unfeasible (cf. Calzado et al.: J. Chem. Phys. 116, 2002, 3985).

Therefore, beginning in the 1980s, several new techniques based mainly on Density Functional Theory (DFT) were developed and applied to solve the problem of calculating multiplet energies and thus to the first principle determination of magnetic spin Hamiltonian parameters. In this work, we will describe three of them, that is: (i) the Broken Symmetry (BS) approach, (ii) the SD method and (iii) the Spin Projection technique. All these methods have been applied to real and to model systems (cf. next section: Application). In case of smaller model systems a comparison to post-HF results are also included.

2.2.2. Quantitative model

2.2.2.1. The broken symmetry approach. The BS approach, developed by Noodleman [18,19] and co-workers, relates the energy of a BS SD, which is not an eigenstate of the $\mathbf{S}^2$, to the energy of a pure spin state.

The most important feature of this technique is that only the calculations of the energy of SDs are needed to approximate the energies of all spin manyfolds. On the other hand, the main limitation is that the method is based on a pure HDVV spin Hamiltonian, thus all non-Heisenberg system will be described incorrectly for this reason.

First, we have to remember that the spin state of highest multiplicity can always be correctly described by a SD. Thus, the energy of the other component of the same multiplicity needed for the calculation of J can easily be obtained.

The BS state is artificially constructed in order to obtain an electronic symmetry which is lower than the actual nuclear symmetry. This is done in order to allow the two magnetic orbitals, which usually belong to different irreducible representations, (e.g. g and u or a and b etc.) to interact by using different orbitals for different spins α and β. The two different orbitals which accommodate electrons with different spins (spin polarised calculation) are usually (vide infra for an extended discussion of this) located on each centre in order to have the maximum local m_S and are coupled together in order to have the minimum resulting $M_{S\mathrm{tot}}$. This corresponds to a globally antiferromagnetic state where the spin α and β density is localised on different paramagnetic centres (Fig. 7).

Noodleman showed that the BS state ($|\psi_B>$) can be approximated by a weighted average of the different

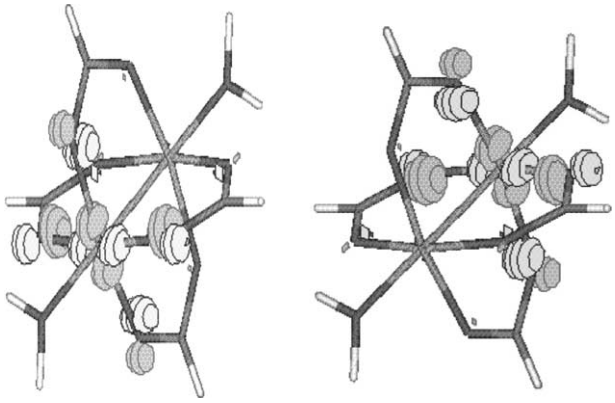

Fig. 7. Broken symmetry α and β component of the HOMO of for diaquatetra-μ-acetato-dicopper(II).

spin state of the system:

$$|\psi_B\rangle = \sum_S \mathrm{A}(S)|\Psi_S \tag{17}$$

Consider two interacting centres A and B and the related, spatially orthogonal, magnetic orbitals a_i and b_i on A and B, respectively. A set of two non-orthogonal orbital $\bar{a}_i = a_i + cb_i$ and $\bar{b}_i = b_i + ca_i$ can be constructed and the overlap between them is therefore $S_{\bar{a}_i\bar{b}_i} = 2c$. If each of the centres has just one unpaired electron occupying the magnetic orbitals a_1 and b_1, the BS determinant reads:

$$\begin{aligned}|\psi_B\rangle &= (N!)^{-1/2}M^{-1/2}\,\det[(a_1 + cb_1)\alpha a_2\alpha \ldots a_n\alpha(b_1 \\ &\quad + ca_1)\beta b_2\beta \ldots b_n\beta] \\ &= (N!)^{-1/2}M^{-1/2}\{\det[a_1\alpha a_2\alpha \ldots a_n\alpha b_1\beta b_2\beta \ldots b_n\beta] \\ &\quad + c(\det[b_1\alpha a_2\alpha \ldots a_n\alpha b_1\beta b_2\beta \ldots b_n\beta] \\ &\quad +)\det[a_1\alpha a_2\alpha \ldots a_n\alpha a_1\beta b_2\beta \ldots b_n\beta] \\ &\quad + c^2\,\det[b_1\alpha a_2\alpha \ldots a_n\alpha a_1\beta b_2\beta \ldots b_n\beta]\}\end{aligned} \tag{18}$$

where, M is the normalisation factor. This determinant can be expressed as the sum of four different contributions:

$$|\psi_\mathrm{B}\rangle = M^{-1/2}(\phi_1 + c(\phi_2 + \phi_3) + c^2\phi_4) \tag{19}$$

Dropping out ϕ_4, which depends on c^2, the other contributions are, respectively, ϕ_1: the purely covalent (A–B)-state, ϕ_2 and ϕ_3: the charge transfer states corresponding to $\mathrm{A}^+\mathrm{–B}^-$ and $\mathrm{A}^-\mathrm{–B}^+$.

The orthonormality condition of ψ_B leads to:

$$\begin{aligned}\langle\psi_\mathrm{B}|\psi_\mathrm{B}\rangle &= \frac{1}{M} \\ &\quad \times [\langle\phi_1|\phi_1\rangle + c^2(\langle\phi_2|\phi_2\rangle + \langle\phi_3|\phi_3\rangle) \\ &\quad + 2c(\langle\phi_1|\phi_2\rangle + \langle\phi_1|\phi_3\rangle)] \\ &= \frac{1}{M}(1 + 2c^2) = 1\end{aligned} \tag{20}$$

therefore, $M = 1 + 2c^2$.

Using the Lowdin and Nesbet spin projection technique, any normalised state ϕ_v can be projected by the ${}^S_{M_S}O$ operator onto its component $|SM_S\rangle$. Therefore, each state can be expressed as:

$$\phi_\mu = \sum_S \sum_{M_S} {}^S_{M_S}O\phi_v \tag{21}$$

Suppose ϕ_v is a Slater determinant constituted by orthonormal orbitals, we then get:

$${}^S_{M_S}O\phi_v = \mathrm{A}_S(S,\ M_s)\left[\phi_v + \sum_\mu \chi_{v\mu}(S,\ M_S)\phi_{v\mu}\right] \tag{22}$$

where $\phi_{\mu v}$ are all the Slater determinants, which can be obtained by a permutation of the spatial part of ϕ_v keeping the spin part constant.

Using the orthogonality theorem for irreducible representations, we obtain:

$$\begin{aligned}&\langle A_v^{-1}{M_S}^S O\phi_v|A_v^{-1}{M_S}^S O\phi_v\rangle \\ &\quad = A_v^{-1}\langle\phi_v|\phi_v + \sum_{\mu=1}^{n'}\chi_{v\mu}\phi_{v\mu}\rangle = A_v^{-1}\end{aligned}$$

$$\langle {}^S_{M_S}O\phi_\mu|H|^{S'}_{M_{S'}}O\phi_v\rangle = \langle\phi_\mu|H|^{S'}_{M_{S'}}O\phi_v\rangle\delta_{SS'}\delta_{MM'} \tag{23}$$

and:

$$\begin{aligned}&\langle {}^S_{M_S}O\phi_\mu|H|^{S'}_{M_{S'}}O\phi_v\rangle \\ &\quad = \mathrm{A}_v\langle\phi_\mu|H|\phi_v + \sum_{\mu=1}^{n'}\chi_{v\mu}\phi_{v\mu}\rangle\delta_{SS'}\delta_{MM'}\end{aligned} \tag{24}$$

The energy of the BS state is, therefore:

$$\begin{aligned}\langle\psi_\mathrm{B}|H|\psi_\mathrm{B}\rangle &= \frac{1}{M}\sum_S \\ &\quad \lfloor\langle\phi_1|H|^S_0O\phi_1\rangle + c^2\langle\phi_2|H|^S_0O\phi_2\rangle \\ &\quad + c^2\langle\phi_3|H|^S_0O\phi_3\rangle + 2c\langle\phi_1|H|^S_0)\phi_2\rangle \\ &\quad + 2c\langle\phi_1|H|^S_0O\phi_3\rangle \\ &\quad \rfloor\end{aligned} \tag{25}$$

where all the element depending on c^2 have been neglected. Finally, we have:

$$\begin{aligned}\langle\psi_\mathrm{B}|H|\psi_\mathrm{B}\rangle &= \frac{1}{M}\sum_S\lfloor A_1(S)\langle\phi_1|\mathbf{H}|\phi_1 \\ &\quad + \sum_\mu \chi_{1\mu}\phi_{1\mu}\rangle + c^2A_2(S)\langle\phi_2|\mathbf{H}|\phi_2 + \sum_\mu \chi_{2\mu}\phi_{2\mu}\rangle \\ &\quad + c^2A_3(S)\langle\phi_3|\mathbf{H}|\phi_3 + \sum_\mu \chi_{3\mu}\phi_{3\mu}\rangle \\ &\quad + 2cA_1(S)\langle\phi_2|\mathbf{H}|\phi_1 + \sum_\mu \chi_{1\mu}\phi_{1\mu}\rangle \\ &\quad + 2cA_1(S)\langle\phi_3|\mathbf{H}|\phi_1 + \sum_\mu \chi_{1\mu}\phi_{1\mu}\rangle\rfloor\end{aligned} \tag{26}$$

where the $A_i(S)$ are the vector coupling coefficients of

the ϕ_i states which can be expressed in terms of S, n and S_{max}.

Let n be the total number of magnetic electrons on the two centres. The resulting state ϕ_1 will be:

$$|S_A S_B\rangle = \left|\frac{n}{2}\ \frac{-n}{2}\right\rangle$$

and

$$A_1(S) = \left[c\left(\frac{n}{2}\frac{n}{2}S;\ \frac{n}{2}\ \frac{-n}{2}\ 0\right)\right]^2$$

where $c(S_A S_B S;\ M_a M_b M)$ is a Clebsh–Gordan coupling coefficient.

Substituting:

$$\frac{1}{M} = \frac{1}{1+2c^2} = 1-2c^2$$

and

$$c^2\langle\phi_v|\mathbf{H}|\phi_v + \sum_\mu \chi_{\mu v}\phi_{\mu v}\rangle \geq E_v$$

and expressing with: $E_1 = \langle\phi_1|\mathbf{H}|\phi_1\rangle$; $E_2 = \langle\phi_2|\mathbf{H}|\phi_2\rangle = E_3 = \langle\phi_3|\mathbf{H}|\phi_3\rangle$, the energy of the BS state becomes:

$$\begin{aligned}\langle\psi_B|\mathbf{H}|\psi_B\rangle &= \langle\phi_1|\mathbf{H}|\phi_1\rangle + \sum_S A_1(S)\left[\frac{n-S(S+1)}{n^2}\right] \\ &\times \sum_{i,j}\left\langle a_i b_j\left|\frac{1}{r_{12}}\right|a_i b_j\right\rangle + \sum_S A_1(S)\left[\frac{n(n+1)-S(S+1)}{n^2}\right] \\ &\times\left\{2S_{\bar{a}\bar{b}}\left[\langle a_1|h|b_1\rangle + \left\langle a_1 b_1\left|\frac{1}{r_{12}}\right|a_1 a_1\right\rangle + \frac{S^2_{\bar{a}\bar{b}}}{2}(E_2-E_1)\right]\right\} \quad (27)\end{aligned}$$

The energy of a pure spin state ψ_S is given as:

$$\psi_S = \sqrt{\frac{M}{M'}}\,{}^S_0 O\psi_B$$

where the normalisation constant M' is:

$$\begin{aligned}M' &= \langle\phi_1|{}^S_0 O\phi_1\rangle + c^2\langle\phi_2|{}^S_0 O\phi_2\rangle + \langle\phi_3|{}^S_0 O\phi_3\rangle \\ &= A_1(S) + 2c^2 A_2(S) \quad (28)\end{aligned}$$

Thus, the energy of a pure spin state is, therefore:

$$\begin{aligned}\langle\psi_S|H|\psi_S\rangle &= \langle\phi_1|H|\phi_1\rangle + \left[\frac{n-S(S+1)}{n^2}\right]\sum_{i,j}\left\langle a_i b_j\left|\frac{1}{r_{12}}\right|a_i b_j\right\rangle \\ &+\left[\frac{n(n+1)-S(S+1)}{n^2}\right]\left\{2S_{\bar{a}\bar{b}}\left[\langle a_1|h|b_1\rangle\right.\right. \\ &\left.\left.+\left\langle a_1 b_1\left|\frac{1}{r_{12}}\right|a_1 a_1\right\rangle + \frac{1}{2}S^2_{\bar{a}\bar{b}}(E_2-E_1)\right]\right\} \quad (29)\end{aligned}$$

From equation (27) and (29) we can see that the energy of the BS state is a weighted average of the energies of pure spin states and it is also a function of $S_{\bar{a}\bar{b}}$, the overlap integral between the magnetic orbitals. Variational minimisation of the energy i.e. imposing that $\frac{\partial E}{\partial S} = 0$ permits one to determine $S_{\bar{a}\bar{b}}$ and the energies of the two states.

The value of $S_{\bar{a}\bar{b}}$, variationally determined from the BS state is equal to the one determined from a pure spin state S, i.e.

$$\begin{aligned}S_{\bar{a}\bar{b}} = 2c &= \frac{2\langle\phi_2|\mathbf{H}|\phi_1\rangle}{E_1 - E_2} \\ &= \frac{2\left[\langle a_1|h|b_1\rangle + \left\langle a_1 b_1\left|\frac{1}{r_{12}}\right|a_1 a_1\right\rangle\right]}{E_1 - E_2} \quad (30)\end{aligned}$$

This means that we will obtain the same result when starting from a BS wavefunction and projecting on a pure spin state S or vice versa.

From a computational point of view the use of BS wavefunctions is particularly convenient because its energy can be obtained through a simple SCF procedure while the energy of any intermediate spin state would need a multiconfigurational procedure.

This feature makes the BS Method very popular for systems with large number of unpaired electrons.

To correlate the energy of the BS state with the HDVV spin Hamiltonian parameters we have just to remember that the energy of the BS state is a weighted average of the energy of the pure spin states. Therefore for a binuclear system AB where $S_A = S_B$ and $S_{max} = S_A + S_B$, we have:

$$\mathbf{H}_{HDVV} = J^{ex}\hat{\mathbf{S}}_\mathbf{A}\cdot\hat{\mathbf{S}}_\mathbf{B}$$

the difference in energy between the highest spin states and the BS states is given by:

$$\begin{aligned}&E(S_{max}) - E_B \\ &= (S_{max}(S_{max}+1) - \sum_{S=0}^{S_{max}} A_1(S)S(S+1))\frac{J}{2} \quad (31)\end{aligned}$$

Using:

$$\sum_S^{S_{max}} A_1(S)S(S+1) = S_{max}$$

we get:

$$E(S_{max}) - E_B = S^2_{max}\frac{J}{2} \quad (32)$$

For binuclear systems where $S_A \neq S_B$ the equation (31) becomes:

$$\begin{aligned}&E(S_{max}) - E_B \\ &= (S_{max}(S_{max}+1) - \sum_{S=n_1}^{S_{max}} A'_1(S)S(S+1))\frac{J}{2} \quad (33)\end{aligned}$$

where $|S_A - S_B| = n_i$, $|S_A - S_B| \leq S \leq S_A + S_B$ and $A'_S = [c(S_A S S; m_A m_B - n_i)]^2$.

Therefore, the following expression can be derived:

$$E(\mathrm{HS}) - E_B = 2J^{ex} S_A S_B \tag{34}$$

All this has been derived by supposing that the magnetic orbitals are orthogonal. Normally, a correction for the overlap between magnetic orbital has to be applied since we are using unrestricted non-orthogonal magnetic orbitals.

In the case of a dimmer, the following, overlap corrected, expression for the J value can be derived:

$$J^{ex} = \frac{E(\mathrm{HS}) - E(\mathrm{BS})}{2S_A S_B(1 + s_{AB}^2)} \tag{34a}$$

where s_{AB} is the overlap between the magnetic orbitals.

This expression yields J-values that can differ by 100% considering the two limits $s_{ab}^2 = 0$ (strong localised limit) or $s_{ab}^2 = 1$ (strongly delocalised orbital). Calculations using both regimes can be found in literature. Some authors, claiming a tendency of DFT to give more delocalised magnetic orbitals with respect to UHF, are commonly assuming the strongly delocalised limit [20].

Malrieu et al. [21] have deeply analysed the effect of the non-orthogonality of magnetic orbitals in the BS approach in the case of reference (HHeH and $[Cu_2Cl_6]^{2-}$) and more complex ($[Cu_2O_{11}]^{18-}$ embedded cluster) systems by explicitly computing S_{ab}^2. Their conclusion is that there is no evidence for assuming a strong delocalised limit, also when using hybrid functionals such as B3LYP, even if in that way nice agreement with experiment is found.

The strong localised limit or, better, the direct evaluation of S_{ab}^2 should be preferred especially in the case where direct interaction can not be neglected.

In the section on applications (vide infra) the strong localised limit was assumed and in one of the examples (BVD radical) a direct evaluation of S_{ab}^2 was performed by monitoring the expectation value of S^2 (see Section 2.2.2.3).

It must be stressed that, beside the fact that almost all the calculation using BS have been done using DFT, there are no theoretical limitations to the use of Unrestricted-HF wave function as well for the same purpose.

Finally, it is worth citing a work of Mouesca [22] where an harmonization of the results obtained for exchange coupling evaluation when using BS and qualitative methods is given.

2.2.2.2. The single determinant method. The SD [23] makes use of the full multi-determinant nature of an open-shell state expressed as a linear combination of Slater Determinants (single determinant (SD)). This is done by using vector coupling (symmetry adaptation of the N-electrons wave function) and yields first order expressions for the multiplet energies consisting of linear combinations of SD energies. In order to calculate these quantities, both spatial and spin symmetry are fully exploited. This method was first developed for the calculation of optical transitions [24], but has also been successfully applied to the study of magnetic properties.

The wave function, ψ_i, of a multiplet whose spatial component belongs to the irreducible representation Γ, component m_Γ, and whose spin part is described through S and m_S i.e. $\psi_i = |\alpha \Gamma m_\Gamma S m_S\rangle$ can be expressed as:

$$\psi_i = \sum_\mu A_{i\mu} \phi_\mu \tag{35}$$

Where the ϕ'_μs are Slater determinants expressed in terms of the spin orbitals χ_i as: $\phi_\mu = |\chi_1 \chi_2 \chi_3 \ldots \ldots|$ and where $A_{i\mu}$ is a square matrix of the expansion coefficients.

The energy of each mono-determinantal state $E(\phi_\mu)$ can directly be obtained from a non-empirical quantum chemical calculation. It is usually convenient to optimise the orbital corresponding to an Average of Configuration (AOC) in a SCF calculation and subsequently to use these frozen orbitals to calculate the energies of the corresponding SD. Neglecting the contribution common to this AOC, the energy of each mono-determinantal state can be expressed in terms of electrostatic two-electrons integrals, as:

$$E(\phi_\mu) = \sum_{p<q} \left[\int \int \chi_p^*(1) \chi_q^*(2) \mathbf{G}_{12} \chi_p(1) \chi_q(2) \mathrm{d}V_1 \, \mathrm{d}V_2 - \int \int \chi_p^*(1) \chi_q^*(2) \mathbf{G}_{12} \chi_p(2) \chi_q(1) \mathrm{d}V_1 \, \mathrm{d}V_2 \right] \tag{36}$$

where $\mathbf{G}_{12} = \dfrac{1}{r_{12}}$.

The two-electron operator $\mathbf{G}_{12}$ can be developed in terms of one-electron operators $g_{k,f\varphi}(1)$ and $g_{k,f\varphi}(2)$ which are equivalent to the solid harmonics $r_1^k Y_{lm}^1(\theta_1 \varphi_1)$ and $r_2^k Y_{lm}^2(\theta_2 \varphi_2)$ used in electronic structure theory of atoms. The resulting expansion reads:

$$\frac{1}{r_{12}} = \sum_{f\varphi} \sum_k g_{k,f\varphi}(1) g_{k,f\varphi}(2) \tag{37}$$

where $g_{k,f\varphi}(i)$ are mono-electronic operator of symmetry f with component φ. The sum k accounts for multiple occurrence of each irreducible representation f.

Hence, the expression for each bi-electronic integral becomes:

$$\langle a\alpha(1)b\beta(2)|\mathbf{G}_{12}|c\gamma(1)\mathrm{d}\delta(2)\rangle = \sum_{k,f\varphi}\langle a\alpha(1)|g_{k,f\varphi}(1)|c\gamma(1)\rangle\langle b\beta(2)|g_{k,f\varphi}(2)|\mathrm{d}\delta(2)\rangle = \sum_{f,\varphi} V\begin{pmatrix} a & c & f \\ \alpha & \gamma & \varphi \end{pmatrix} V\begin{pmatrix} b & d & f \\ \beta & \delta & \varphi \end{pmatrix} \times \sum_{k}\langle a||g_k||c\rangle\langle b||g_k||d\rangle \quad (38)$$

$V\begin{pmatrix} \cdot & \cdot & \cdot \\ \cdot & \cdot & \cdot \end{pmatrix}$ are the V-coefficients of Fano and Racah, related to the $3j$ as:

$$V\begin{pmatrix} j_1 & j_2 & j \\ m_1 & m_2 & -m \end{pmatrix} = (-1)^{j_1+j_2+j}\begin{pmatrix} j_1 & j_2 & j \\ m_1 & m_2 & -m \end{pmatrix} \quad (39)$$

We define reduced bielectronic matrix element $R(ab, cd, f)$ the sum over k of the monoelectronic reduced matrix elements:

$$R(ab,\ cd,\ f) = \sum_{k}\langle a||g_k||c\rangle\langle b||g_k||d\rangle \quad (40)$$

For symmetry reason the matrix elements $\langle m||g_l||n\rangle$ are different from zero if and only if $m \otimes n \in l$. Moreover, if $m = n$, l is restricted to the symmetrized square: $[m \otimes n]_{\mathrm{sym}}$.

The energy of a SD $E(\phi_\mu)$ is, therefore:

$$E(\phi_\mu) = \sum_{\rho=1}^{N} B_{\mu\rho}R_\rho \quad (41)$$

where $B_{\mu\rho}$ is a rectangular $m \times n$ matrix where m is the number of microstates which belongs to this configuration, and n is the number of the electrostatic reduced matrix elements which can be defined in the space of the spinorbitals $\chi_1\chi_2\ldots\chi_n$ which contributes to the μ-th microstate (SD).

B can be reduced to a full rank matrix $U(\mu_i, j)$ which relates m microstates ϕ_μ to a subset of r ($r < m$) non-redundant $\phi_{\mu i}$.

In terms of non-redundant microstates we get:

$$E(\phi_\mu) = \sum_{j=1}^{r} C_{\mu j}E(\phi_{\mu j}) \quad \mu = 1,\ \ldots,\ m \quad (42)$$

$$R_\rho = \sum_{j=1}^{r} D_{\rho j}E(\phi_{\mu j}) \quad \rho = 1,\ \ldots,\ n \quad (43)$$

Finally the energy of each multiplet ψ_i can be expressed as:

$$E(\psi_i) = \langle\psi_i|G|\psi_i\rangle = \sum_{j=1}^{r} F_{ij}E(\phi_{\mu j}) \quad (44)$$

The energy of a multi-determinantal spin state (ψ_i) can be finally expressed as a linear combination of energies of SDs. The higher is the symmetry the greater is the performance of the method because the number of non-redundant microstates decreases significantly.

Some approximations and limitations in the practical implementation of the method are:

a) The method does not consider the two-electron second order terms, which are neither exchange nor coulomb, and which cannot, in general, be expressed in terms of energies of SDs but involve off-diagonal elements $\langle\Phi_\mu|G|\Phi_\nu\rangle$.
b) The method is usually applied within the active electrons approximation. In this case it is possible to include second order electrostatic interaction exactly (vide infra). Hence, frequently, only the microstates arising from different occupations of the active orbitals are taken into account.

In order to illustrate the method, let us consider two metal centres A and B with one unpaired electron on each, interacting through the doubly occupied orbitals of a diamagnetic bridging ligand X (super-exchange). The following interaction diagram can be drawn Fig. 8.

Considering just the Semi-Occupied Molecular Orbitals (SOMO) as active orbitals, four multiplets will occur, i.e. $|a^{21}A\rangle$; $|b^{21}A\rangle$; $|ab^{1}B\rangle$; $|ab^{3}B\rangle$.

Applying the energy decomposition as explained in the text we obtain the following scheme Fig. 9.

It is easy to notice that the energy of each state is expressed just in terms of the energy of a SD and that the configuration interaction of state with the same symmetry (^{1}A) is also taken into account as a second order correction.

2.2.2.3. The spin projection technique. The Spin Projection technique presented here was developed by Ovchinnikov and Labanowski [25]. These authors present the problem of Spin Contamination, already known for HF calculation, in a general formalism, which can also be applied to DFT calculations. It is important to underline that this topic is presently the subject of much debate. We can easily assume that the spin-state of

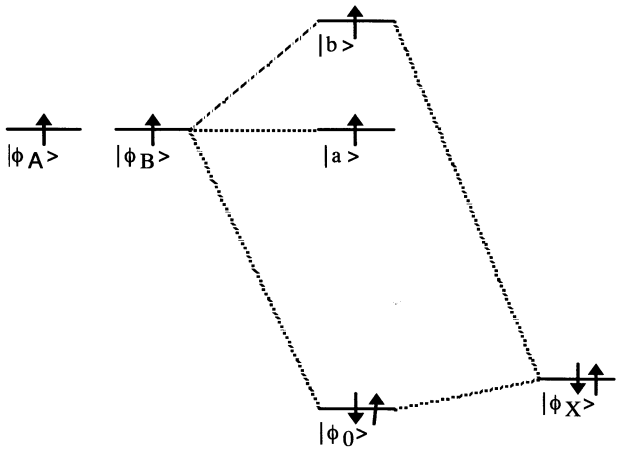

Fig. 8. Interaction diagram for an A–X–B molecule.

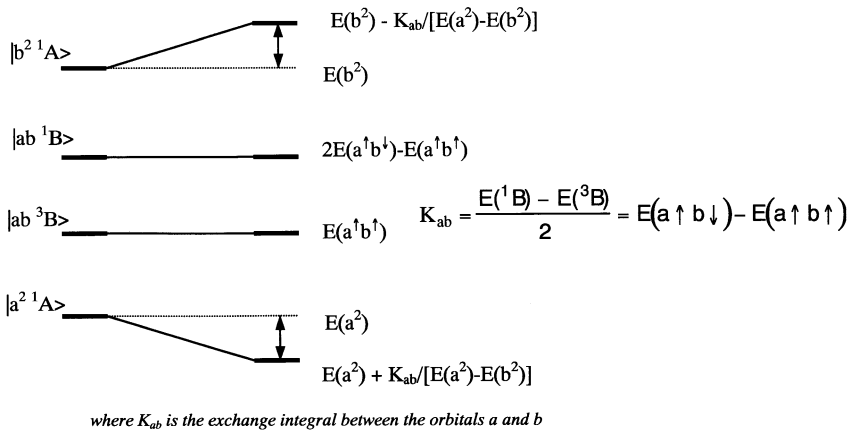

Fig. 9. Multiplet energies in term of single determinants.

highest multiplicity is almost a pure one and that it can be represented by a SD. Whereas the lower spin states are usually contaminated by the higher spin state components of the same M_S-value.

Let us first consider the easiest case i.e. a binuclear system with one unpaired electron per site. Two different total spin states can arise i.e. a singlet (S) and a triplet (T).

Any unrestricted wavefunction $\psi_{\mathrm{unr},S}$ with $M_S = 0$ can be expressed as a linear combination of pure singlet and triplet spin states as:

$$\psi_{\mathrm{unr},S} = a\psi_{\mathrm{S}} + b\psi_{\mathrm{T}} \tag{45}$$

with: $a^2 + b^2 = 1$

Thus, if we apply the total spin operator S^2 to both sides of equation 45 we generate the following expression for b^2:

$$b^2 = \frac{1}{2}\langle\psi_{\mathrm{unr},S}|S^2|\psi_{\mathrm{unr},S}\rangle \tag{46}$$

Applying also the Hamilton operator to both sides again we get:

$$\begin{aligned} E_{\mathrm{unr},S} &= \langle\psi_{\mathrm{unr},S}|\mathbf{H}|\psi_{\mathrm{unr},S}\rangle \\ &= a^2\langle\psi_{\mathrm{S}}|\mathbf{H}|\psi_{\mathrm{S}}\rangle + b^2\langle\psi_{\mathrm{T}}|\mathbf{H}|\psi_{\mathrm{T}}\rangle \end{aligned} \tag{47}$$

Hence, the energy of the pure singlet state can be expressed as:

$$E_S = \frac{E_{\mathrm{unr},S} - b^2E_{\mathrm{T}}}{1 - b^2} \tag{48}$$

and the difference in energy between the singlet and the triplet is:

$$\Delta_{\mathrm{ST}} = E_{\mathrm{S}} - E_{\mathrm{T}} = \frac{E_{\mathrm{unr},S} - E_{\mathrm{T}}}{1 - b^2} \tag{49}$$

This approach can be generalised for any spin system. Considering a system where the maximum spin state is $S_{\max}$, any unrestricted wavefunction with $M_S = S_i$, where S_i is an intermediate spin state, will be described as:

$$\begin{aligned} \psi_{\mathrm{unr},S_i} &= a_{S_i}(S)\psi_S + a_{S_i}(S+1)\psi_{S+1} + \ldots \\ &\quad + a_{S_i}(S_{\max})\psi_{S\max} \end{aligned} \tag{50}$$

Applying the operator:

$$B_L = (S^-)^L(S^+)^L$$

to the left hand side of the equation above we get:

$$\langle\psi_{\mathrm{unr},S_i}|B_L|\psi_{\mathrm{unr},S_i}\rangle = L!\sum_{j,j'=1}^{L}\det[V(j,\ j')] \tag{51}$$

where the V matrix is defined as:

$$V(j,\ j') = \delta_{j,j'} = \sum_k s_{jk}^{\alpha\beta}s_{j'k}^{\alpha\beta}n_k^{\beta} \tag{52}$$

For the right hand side of the same equation we can use the properties of the spin ladder operator to obtain the following expression:

$$\begin{aligned} &\langle\psi(S,\ M)|B_L|\psi(S,\ M)\rangle \\ &\quad = \prod_{i=0}^{L-1}[S(S+1) - (M+1)(M+i+1)] \end{aligned} \tag{53}$$

Defining:

$$T_K(P,\ S) = \prod_{i=0}^{P-1}[S(S+1) - (K+i)(K+i+1)] \tag{54}$$

yielding the following set of equation:

$$\begin{aligned} &A_{S_i}(S) + A_{S_i}(S+1) + A_{S_i}(S+2) + \ldots + A_{S_i}(S+L) = 1 \\ &T_{S_i}(1,\ S+1)A_{S_i}(S+1) + T_{S_i}(1,\ S+2)A_{S_i}(S+2) + \ldots \\ &+T_{S_i}(1,\ S+L)A_{S_i}(S+L) \\ &= B_1 \ldots\ldots T_{S_i}(L,\ S+L)A_{S_i}(S+L) = B_L \end{aligned} \tag{55}$$

where: $A_{S_i}(S) = a_{S_i}(S)^2$

The solution of this linear system of equations yields the $A_{S_i}(S)$ coefficient and therefore the mixing of the

pure spin state into the unrestricted wavefunction. The energy of each intermediate pure spin state is thus:

$$E_{\mathrm{corr}}(S) = \frac{E_{\mathrm{uncor}}(S) - A_{S_i}(S+1)E_{\mathrm{corr}}(S+1) - A_{S_i}(S+2)E_{\mathrm{corr}}(S+2) - \ldots}{1 - A_{S_i}(S+1) - A_{S_i}(S+2) - A_{S_i}(S+3) - \ldots} \quad (56)$$

A final remark concerning the formula derived for the singlet-triplet energy difference: it is easy to prove that the BS (formula 34a) and the Spin projection formalism (formula 49) are exactly identical for this case.

2.3. An illustrative example: the H_2 molecule

The H_2 molecule, at long inter atomic distance, presents two unpaired electron, one on each centre, and the interaction between these two electrons can be considered as an example of magnetic interaction. We can therefore analyse the behaviour of the different spin states, i.e. the triplet with $S = 1$ and the singlet with $S = 0$ as a function of the inter-atomic distance. This example has all the ingredients of a molecular magnet and all the computational concepts introduced so far will be illustrated and become clear.

Fig. 10 represents the dissociation curve for the H_2 molecule as computed in a minimal basis set, full-CI, treatment

As expected, the triplet-state is always higher in energy with respect to the lowest singlet and their respective energies become identical at long distance, where the interaction between the centres is negligible. This situation is in full agreement with the qualitative semi-empirical rules outlined in Section 2.2.1.

If we consider just the singlet ground state, then the full CI result can be compared with a Restricted HF (RHF) and a Restricted DFT/LDA (RDFT/LDA) calculation (cf. Fig. 11). By restricted we mean that two electrons with different spins α and β do occupy the same spatial orbital. The horizontal mirror symmetry (D_{8h}) of H_2 requires that the two magnetic orbitals belong to two different irreducible representations: σ_g^+ and σ_u^+. By unrestricted, on the contrary, we mean that the spatial shape of orbitals which do accommodate α- and β-electrons are free to relax i.e. the horizontal

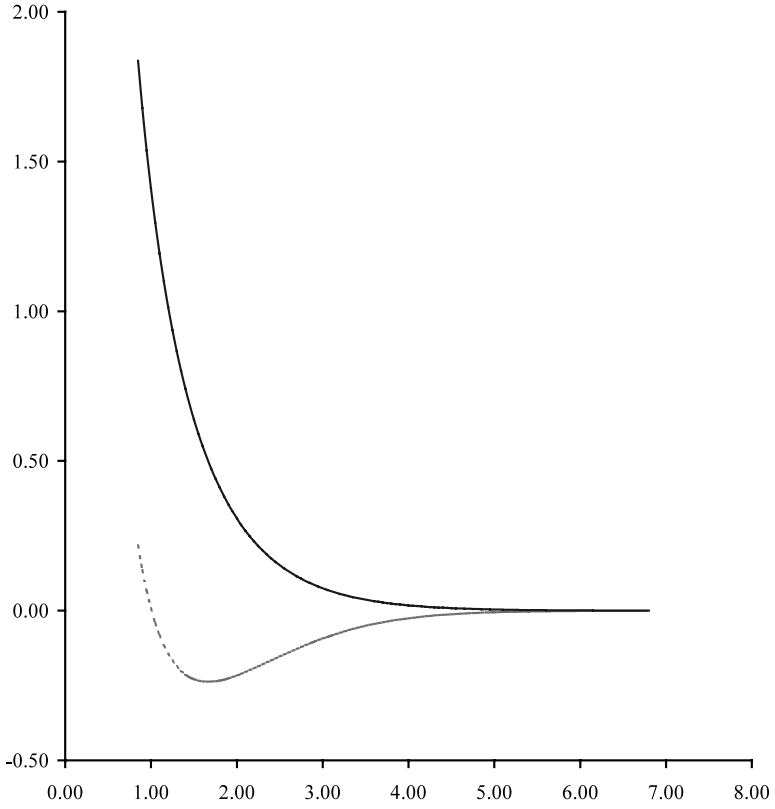

Fig. 10. Dissociation energy curves for the triplet and lowest energy singlet of H_2 molecule.

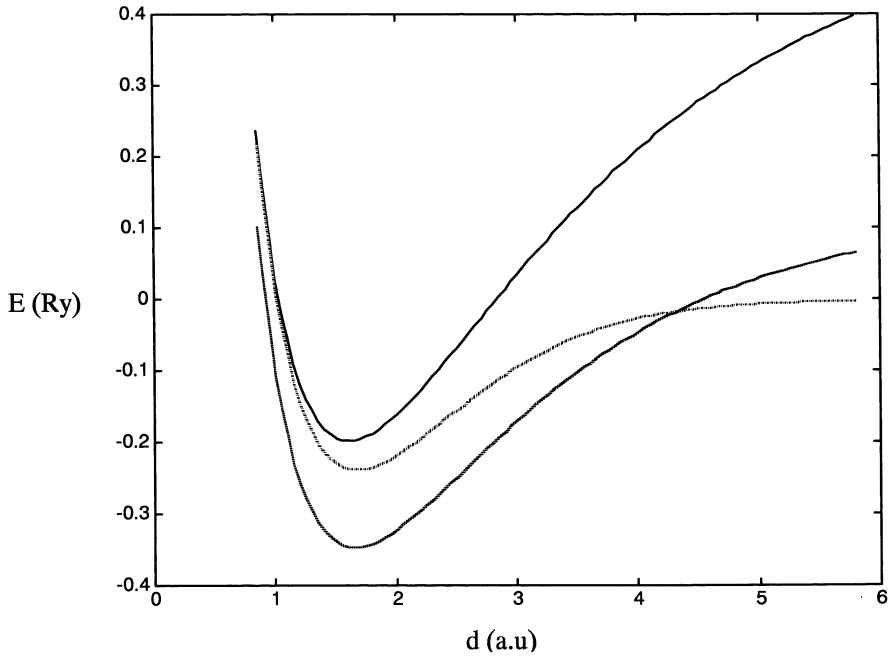

Fig. 11. Full-CI (dot-dashed line) vs. RHF (full line) and RDFT–LDA (dashed line) energies for the lowest energy singlet state of H_2 as a function of the intermolecular distance.

mirror plane of H_2 is artificially removed (BS: $D_{8h} \rightarrow C_{8v}$) and the orbitals which now do interact, are individually optimised according to the variational principle.

Of course the dissociation behaviour is not correctly reproduced because of the restricted SD approximation. However the singlet–triplet separation, for which the correct behaviour is to vanish when the inter-atomic distance increases, is much closer to reality for the RDFT-curve than for the RHF-curve. This behaviour is of course related to near degeneracy correlation, which is much better reproduced in DFT than in HF calculations. We can also comment on the well known over-binding feature observed for the LDA calculation, i.e. the minimum RDFT is too low.

In order to properly describe the long-range behaviour of the dissociation curve, an unrestricted formalism must be used. The role of correlation energy must also be considered.

The so-called dynamical correlation i.e. the instantaneous correlated electrons motion is already included if one uses DFT, whereas the so-called near degeneracy correlation is not. This is the reason why in Fig. 12 the corrected asymptotic behaviour is observed for both, the BS and the SD method where near degeneracy correlation is partially taken into account (in fact completely at infinite separation). It is also interesting to notice that in this case the BS behaviour is the closest to the full-CI one.

Moreover, the different behaviour of the RDFT versus the UDFT at long range can be related to the extra degree of freedom allowing for localisation of the spin α and β on different centres in the unrestricted calculation. This can easily be shown by monitoring $\langle S^2 \rangle$ as a function of distance (cf. Fig. 13). The calculation of $\langle S^2 \rangle$ is analogous to the spin decontamination described in Section 2.2.2.3.

It can easily be seen that localisation takes places for $\langle S^2 \rangle > 0$, as soon the RDFT and UDFT curves start to differ.

This terminates our methodological part. We also hope that the experimentalists are now confident about the computational tools involved in the coming section.

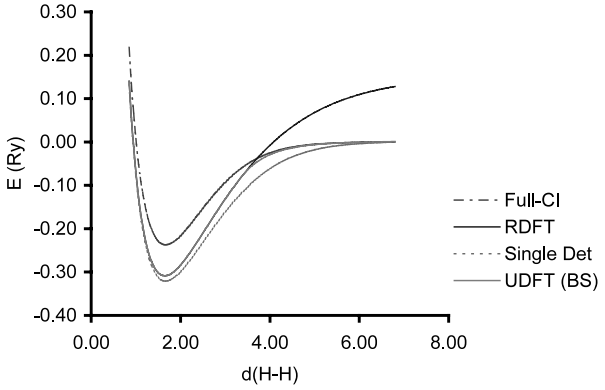

Fig. 12. Full-CI vs. RDF, UDFT and SD energies for the lowest energy singlet state of H_2 as a function of the intermolecular distance.

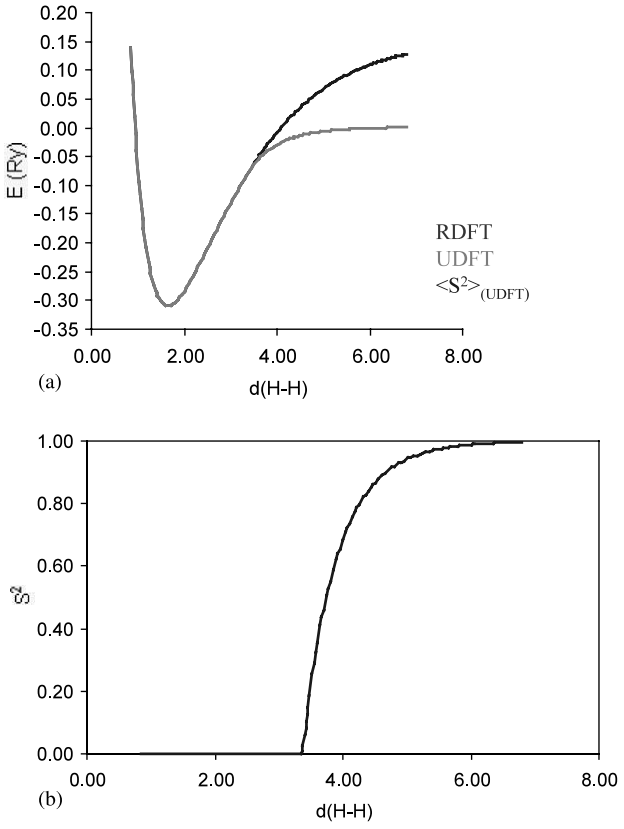

Fig. 13. (a) RDF and UDFT for the lowest energy singlet state of H_2 as a function of the intermolecular distance. (b) $\langle S^2 \rangle$ for the UDFT calculation as a function of the intermolecular distance.

3. Applications

Some typical applications of DFT to model systems and to real paramagnetic systems are reported. As soon as the dimensions of the systems increase, less demanding techniques have been applied and instead of a comparison to sophisticated post-HF calculations, direct comparison with the experimental values is given.

Concerning the model systems, two kind of examples were considered: the HHeH and the $[Cu_2Cl_6]^{2-}$. The first one (HHeH) is a perfect candidate to study the exchange interaction between two paramagnetic sites (the H atoms) through a diamagnetic bridging ligand (the He atom), in the simplest possible way. The $[Cu_2Cl_6]^{2-}$ system has been used in experimental and theoretical work to understand the magnetic interactions between two metallic paramagnetic sites and the effect of structural deformations (magneto-structural correlations).

In the case of real systems: i.e. $Ti(CatNSQ)_2$, $Sn(CatNSQ)_2$ or BVD (vide infra), due to the dimension of the systems, extensive post-HF treatments were not possible and a structural modeling was performed. The calculated values are directly compared with the experimental ones.

Finally, an example of the possible extension to mixed valence systems is given in the case of the well characterized $[Fe_2(OH)_3(tmtacn)_2]^{2+}$ and $[Cu_3O_2L_3]^{3+}$ complexes.

3.1. Technical details

For the sake of clarity the following notation is used throughout in order to specify the different approaches: CAS(n, m), complete active space multiconfigurational SCF post HF calculations involving a set of m orbitals with n electrons; QCISD(T), quadratic CI including single, double and triple perturbative substitutions; BS, BS assuming the strongly localised limit $S^2_{ab} = 0$ (vide infra); SD, SD (vide infra); RU-, using ROHF wave function; PU-, using projected UHF triplet energies.

The effect of the different exchange-correlation functionals used for the computed exchange coupling constant was also studied. The following notation is used: Xα, Slater's modification of Dirac's local exchange ($\alpha = 0.7$) [26]; VWN, Dirac's local density approximation for exchange and Vosko, Wilk and Nusair's expression for correlation energy of a uniform electron gas [27]; VWN+Stoll; same as VWN plus the Stoll's local correction to correlation [28]; BP, gradient corrected functional combination of Becke's gradient corrected exchange functional [29] and Perdew's correlation functional [30]; PW91, gradient corrected exchange and correlation functional proposed by Perdew and Wang [31]; BLYP, gradient corrected functional combination of Becke's gradient corrected exchange functional [30] and Lee, Yang and Parr's correlation functional [32]; B3LYP, hybrid functional including exact HF exchange in the ratio proposed by Becke [33].

If not differently specified HF and post-HF calculations or calculation involving hybrid exchange correlation functionals, were performed using GAUSSIAN 94 [34]. All other DFT calculations were performed using the ADF program package [35] (Version 2.01 to ADF2000.02). The basis sets used are specified in the text or in the corresponding references.

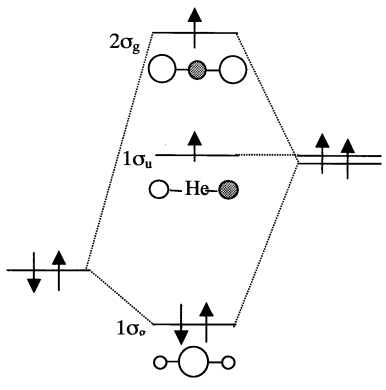

Fig. 14. One electron energy level diagram for H–He–H.

Table 1
Singlet–triplet energy differences (in cm^{-1}) computed for H–He–H at different H–He distances

	H–He distance (Å)		
Method	1.25	1.625	2.00
Ab initio [a]			
CAS (2, 2)	4204	476	48
OVB-MP2 (2, 2)	4358	420	26
CAS (4, 3)	4294	484	46
OVB-MP2 (4, 3)	4530	492	48
QCISD (T)	4928	790	202
RU-BS	4298	526	60
PU-BS	4580	554	60
Full CI	4860	544	50
DFT[b]			
Xα BS	6004	646	58
LDA-BS	12 432	760	158
BP-BS	10 529	1268	134
Xα-SD	5631	745	64
LDA-SD	9050	1553	183
BP-SD	7799	1170	123

[a] 6-311G** basis set.
[b] Standard ADF triple-ζ Slater type basis set.

3.2. Model systems[3]: HHeH and $[Cu_2Cl_6]^{2-}$

Amongst the possible model systems, which can be designed in order to mimic the main interaction involved in a super-exchange pathway, the linear H–He–H molecule is certainly the simplest. The different spin states arise from the distribution of three electrons in four different orbitals, as schematically depicted in Fig. 14.

Due to its size, this molecule can be fully characterized at an ab-initio post-HF level and therefore it has been chosen as benchmark for the DFT techniques.

The $^1\Sigma_g^+$ is predicted to be the ground state and the lowest triplet state is the $^3\Sigma_u^+$.

In Table 1 the computed energy differences between the triplet and the singlet states are reported for three different H–He distances. Ab initio calculations were performed with the programs GAMESS [37], GAUSSIAN 94 [34] and HONDO-CIPSI [38].

All the techniques are able to reproduce the correct singlet ground state and the variation of the singlet–triplet energy gap as a function of the distance, which can be considered as a very simple example of 'magneto-structural correlation'. Assuming the full-CI results as the exact value (they are in agreement with previous calculation by Hart et al. [39]), it easy to notice that the CAS(2,2) approach is in reasonably good agreement with the exact results, showing that a fairly large part of correlation is taken in to account already at this level. On the other hand, due probably to the spin contamination of the reference wavefunction, the QCISD(T) approach does not lead to results of the same quality. The BS approach, especially when using HF wavefunction, gives results in good agreement with the full-CI calculations. Regarding DFT based calculations, an overestimation of the singlet–triplet energy gap is found especially when going from Slater Xα exchange only functional to local or gradient corrected exchange and correlation functionals using both the SD and BS approaches. In any case the correct order of magnitude of the splitting is reached although we can not say that the results are quantitatively correct.

In the case of BS calculations, Malrieu et al. [21] have shown that when including a correction for overlap between the magnetic orbital better agreement with post-HF data can be found, the effect being larger the shorter the H–He distance, as expected.

Several magneto structural correlation studies have been experimentally established for $[Cu_2Cl_6]^{2-}$ [40,41] therefore this molecule is an optimal candidate for testing the performance of the different computational models. A schematic sketch of the molecule is depicted in Fig. 15.

The results in best agreement with the experiment are those obtained by variational CI calculations of the singlet–triplet energy gap through a judiciously chosen post-HF procedure [42]. These results are collected in Table 2 as LOC and DELOC, corresponding to the use of localized or delocalized molecular orbitals, respectively.

The BS approach reproduces correctly the order of the singlet and of the triplet states, however not the magnitude of the splitting. The SD on the other hand shows the poorest agreement. This is probably due to a lack of description of correlation for the singlet state in the case of the latter approach.

3.3. Real systems

As a matter of fact, it is important to stress the importance of geometrical parameters in the determination of the magnetic properties of all the systems. Therefore, modeling and neglecting the environmental influences e.g. solvent-effects or crystal packing can strongly affect the final results [44]. This is the reason why, when possible, magneto-structural correlations are often investigated and why it is important to reduce to a minimum the modelisation when direct agreement between the experimental and theoretical data is sought. An example of a possible model of a complex molecular magnetic system, within the QM/MM framework, and the effect of modeling on the J values are reported here in the case of the $[Cu_3O_2L_3]^{3+}$ complex.

[3] For a more detailed discussion of the model systems' results address to the original paper [36].

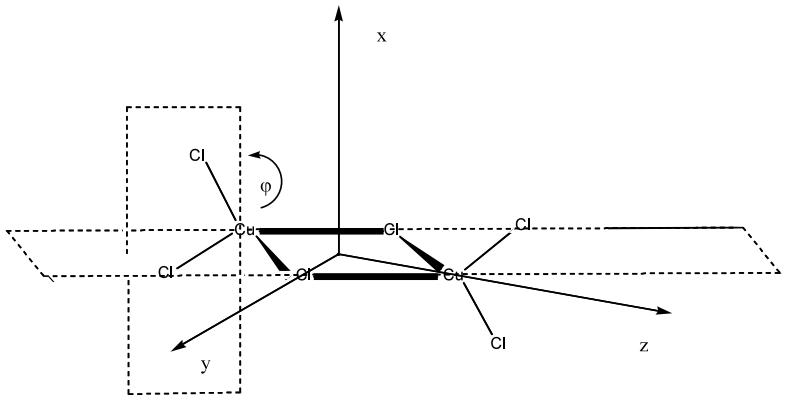

Fig. 15. Schematic structure of $[Cu_2Cl_6]^{2-}$.

Table 2
Singlet–triplet energy differences (in cm^{-1}) computed for $[Cu_2Cl_6]^{2-}$ [c]

Method	φ (°)		
	0	45	70
Ab initio [a]			
Localized [d]	36	−58	87 [e]
Delocalized [d]	6	−47	75 [e]
ROHF-BS	1620	1331	1901
DFT [b]			
Xα SW-BS [f]	198	−210	113
Xα BS	122	−309	72
LDA-BS	362	−246	191
BP-BS	256	−200	109
Xα-SD	−41	−437	−106
LDA-SD	160	−374	45
BP-SD	−35	−402	−145
Experimental	0–40[g]	−80 to −90[h]	–

[a] Basis Set: Hay–Wadt basis set was used for Cu and terminal Cl atoms. The core orbitals were treated using the appropriate pseudo-potential. The bridging Cl atoms were described using a 6-311G all-electron basis set. A p polarisation function was applied to all Cl atoms.
[b] Standard ADF double-ζ basis set was used for Cu and Cl atoms. Orbitals up to 2p for Cu and Cl atoms were kept frozen.
[c] For geometrical parameters see [36].
[d] From [42].
[e] Computed for $\varphi = 90°$.
[f] From [43].
[g] From [40].
[h] From [41].

3.3.1. *Ti(CatNSQ)₂ and Sn(CatNSQ)₂*[4]

These molecules can be considered to be typical examples of interaction between two paramagnetic radical ligands through a formally diamagnetic d^0 Ti^{4+} or Sn^{4+} metal ion. The structure and the magnetic properties of both systems have been fully characterized experimentally [45]. Surprisingly enough, the interaction is ferromagnetic as measured by magnetic susceptibility as a function of temperature. From recent calculations [46], it has been shown that the empty metal orbitals provide an efficient super-exchange pathway between the two radical ligands whose unpaired electron is mainly localized on the donor N atoms. Since the magnetic orbitals are practically orthogonal, an overall ferromagnetic interaction is determined. A significant amount of metal density is, in any case, found in the magnetic orbitals (up to 4%). These results are in agreement with recent neutron diffraction data [47].

The energy of the lowest spin states was computed for a model system (Fig. 16) were the *tert*-butyl groups were substituted by H (see reference [46] for a detailed description) within the SD formalism.

Using this approach, the energy of the $^3A_2$, of the $^1A_2$ and of the $^2A_1$ states arising from different occupations of the magnetic orbitals (of symmetry b_1 and b_2) can be expressed as:

$$E(^3A_2) = E|b_1^+ b_2^+|$$

$$E(^1A_2) = 2E|b_1^+ b_2^-| - E|b_1^+ b_2^+|$$

And the energies of two $^1A_1$ come from the diagonalisation of the following 2×2 matrix:

$$E(^1A_1) = \begin{vmatrix} E|b_1^+ b_1^-| & E|b_1^+ b_2^-| - E|b_1^+ b_2^+| \\ E|b_1^+ b_2^-| - E|b_1^+ b_2^+| & E|b_2^+ b_2^-| \end{vmatrix}$$

The results are shown in Table 3.

An excellent, but probably fortuitous, agreement with the experimental data was obtained for the Ti complex while the Sn complex shows the usual reasonable, but semi-quantitative, agreement with the magnetic data.

Nevertheless, it is interesting to see how relatively cheap calculations can give a clear, although not fully quantitative, insight on the mechanism of magnetic interaction on real complex systems.

3.3.2. *BiVerDazyl (BVD) biradical*

Very few examples of stable ferromagnetic free radicals, e.g. galvinoxyl [48], nitroxides [49], nitronyl-

[4] CatNSQ = (3,5-di-*tert*-butyl-1,2-semiquinonato 1(2-hydroxy-3,5-*tert*-butyl-phenyl)immine).

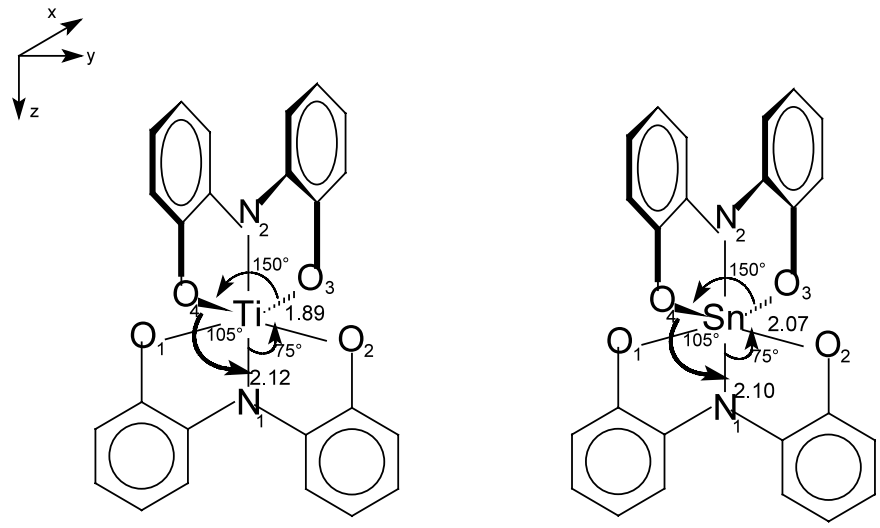

Fig. 16. Schematic structure and main geoemtrical parameters of $Ti(CatNSQ)_2$ and $Sn(CatNSQ)_2$ model systems.

Table 3
Computed energy splitting (in cm^{-1}) for $Ti(CatNSQ)_2$ and $Sn(CatNSQ)_2$ [a]

State	Ti	Sn
$^3A_2$	0.0	0.0
$^1A_2$	57 [56(1)]	58 [23(1)]
$^1A_1$	9510	11 934
$^1A_1$	9571	11 991

The experimental values are reported in square brackets.

[a] Standard ADF triple-ζ basis set was used for Ti and Sn atoms. A standard ADF double-ζ basis set was used for N, C, O and H atoms. Electrons up to 3p for Ti and 4p for Sn and up to 1s for C and N atoms were kept as frozen core. For a complete description of the model used see [43].

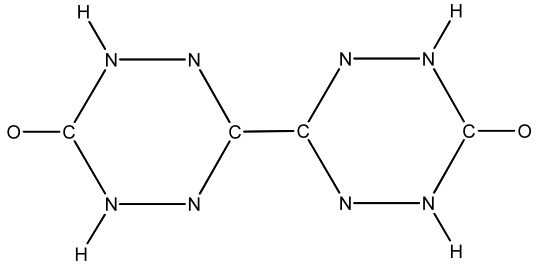

Fig. 17. Schematic structure of BVD model system.

nitroxides [50], and bi-nitroxides [51], have been studied so far experimentally and characterized theoretically [52]. The interest for stable organic radicals that can exhibit ferromagnetic ground states upon chemical functionalization is therefore increasing. BVD is a biradical whose constituting radical moieties (verdazyl [53]) are antiferromagnetically coupled to give a singlet ground state. A schematic representation of the model used in the calculation is given in Fig. 17. The Singlet–Triplet energy gap has been experimentally determined by ESR measurements [54]. The Triplet lies 887 cm^{-1} higher in the crystal and 760 cm^{-1} higher in solution.

The structural, spectroscopic and magnetic properties of this oxo-verdazyl bi-radical have been studied using a model complex were the methyl groups have been substituted by H [55]. DF calculations were performed using GAUSSIAN 94 [34] within the framework of the BS approach explicitly taking into account the correction for the overlap of the magnetic orbitals. The effect of the environment on the tuning of magnetic and structural characteristics of biverdazyls was analyzed by applying the Polarizable Continuum Model (PCM) [56].

The Free Rotor Model was used through out. Therefore, for each inter-ring torsion angle (α) a full geometry optimization of the triplet state was performed. On each optimized geometry a SCF calculation of the BS state was done and the singlet–triplet energy gap determined. The J^{ex} computed value (in cm^{-1}) for different model chemistry is shown in Fig. 18 as a function of the α angle.

Since the difference in energy between the conformation with α smaller than the equilibrium value is small, at room temperature all these conformations can be populated. Therefore, a vibrational average over large amplitude motions was performed in order to obtain a correct J^{ex} value using the following expression:

$$\langle J^{ex}\rangle_T = J^{ex}_{min} + \frac{\sum_j \langle j|\Delta J^{ex}|j\rangle e^{[(E_0-E_j)/kT]}}{\sum_j e^{[(E_0-E_j)/kT]}}$$

The final results including both solvent and vibrational average are presented in Table 4.

Although in this case direct solvent effects are negligible the effect of solvation on the structure is not. The results obtained for the computed singlet triplet splitting are in quantitative agreement with the experi-

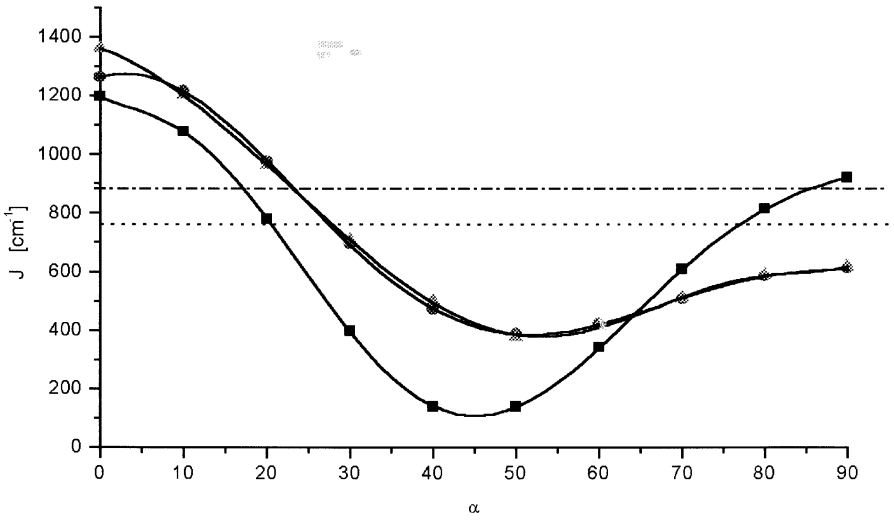

Fig. 18. Computed depence of J^{ex} on the inter-ring torsion angle, α. PCM/B3LYP (●); vacuo/BLYP (■); vacuo/B3LYP (▲). Experimental value in frozen $CHCl_3$ solution (···) and in solid state (–·–) are reported for comparison.

Table 4
Equilibrium angle (α_{min}) and corresponding J^{ex} value (J^{ex}_{min}), and vibrationally avaraged J^{ex} values at 0 and 298 K for BVD (units: cm^{-1} and °) [a]

	Vacuo [b]	$CHCl_3$
α_{min}	34.6	26.8
J^{ex}_{min}	566 (606)	757
$\langle J^{ex}_{min}\rangle$0 K	585 (601)	774
$\langle J^{ex}_{min}\rangle$298 K	721 (729)	844
	Crystal	Solution
Experimental [c]	887	760

[a] Basis set: 6-31G*.
[b] The values in parentheses have been obtained using the geometries computed in vacuo and J computed in $CHCl_3$.
[c] From [54].

mental data. Furthermore the increase of J value with increasing polarity of the environment (i.e. going from vacuo to $CHCl_3$) is in agreement with the experimental observation (i.e. going from solution to crystal). A detailed description of the results and a characterization of the monomer are given in the original paper [55].

3.3.3. $[Fe_2(OH)_3(tmtacn)_2]^{2+}$ [5]

This complex is an example of a mixed valence system where the two iron centres (namely a Fe(III) d^5 and an Fe(II) d^6) are completely equivalent from an experimental point of view both on the long time scale (X-ray) and on short time scale (Mössbauer) [57,58]. This complex is often referred to as a Class III complex in Robin–Day classification [59]. Because valence electron delocalisation between the metal centre is possible, a spin Hamiltonian taking into account not only exchange

[5] Tmtacn = trimetyltriazacyclononane.

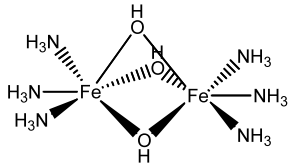

Fig. 19. Schematic structure of the model system $[Fe_2(OH)_3(NH_3)_6]^{2+}$.

but also the double-exchange terms have to be considered. From a magnetic point of view it has $S = 9/2$ high spin as ground state and the difference in energy between the ground and the first $S = 7/2$ excited state was evaluated as 720 cm^{-1}. The experimental J^{ex} value was determined as $J < 235$ cm^{-1} and the B parameter was determined, from UV–vis spectra, as $B = 1350$ cm^{-1} [58].

The BS approach was applied in the modification needed to taken into account the double exchange interaction [60]. A model complex, schematically depicted in Fig. 19, where each tmtacn macrocyclic ligand was substituted with $3NH_3$ molecules was used in all the calculation [61].

The computed J^{ex} and B values are 137 and 1369 cm^{-1}, respectively, which nicely compare with the experimental data. From the constructed spin ladder (shown in Fig. 20) the splitting between the ground and first excited spin state can be evaluated as 752 cm^{-1} in good agreement with the experimental value (720 cm^{-1}).

Furthermore to fully characterise the system an analysis of the PES along a simulated normal coordinate corresponding to the anti-symmetric breathing motion was performed (see ref. [61] for detailed description). This motion is usually referred to as the active normal mode for electron delocalisation [62]. Therefore, the

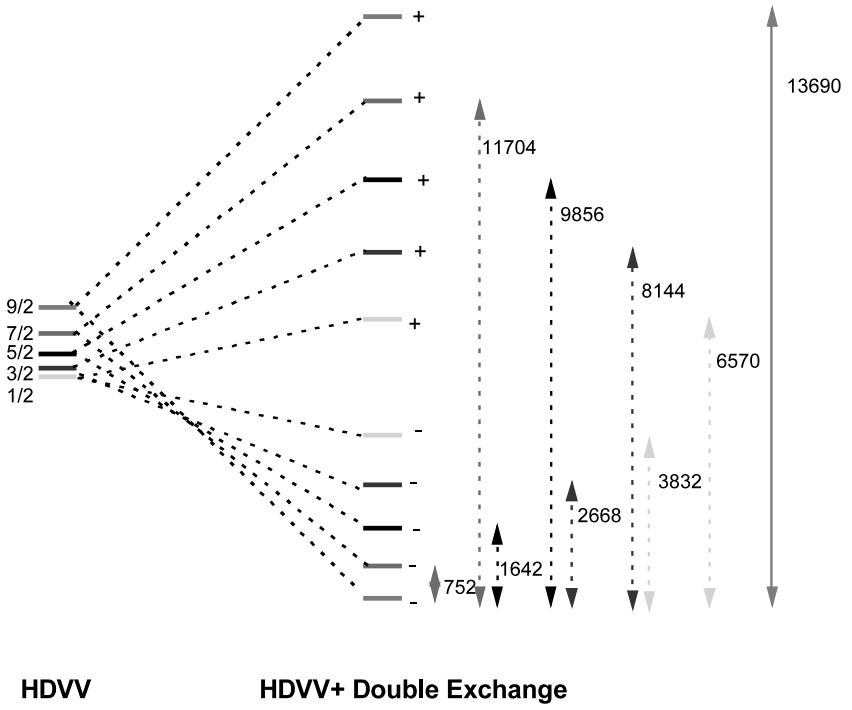

Fig. 20. Computed spin ladder for $[Fe_2(OH)_3(NH_3)_6]^{2+}$.

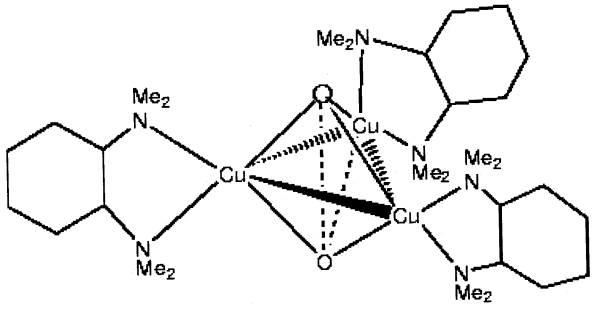

Fig. 21. Schematic structure of $[Cu_3O_2L_3]^{3+}$, L = *N*-permethylated

presence of a single minimum in this surface corresponding to the symmetric structure of the metallic sites is consistent with a fully delocalised picture of the complexes (Class III). From the analysis of the computed PES (see ref. [61]) an estimate of the corresponding harmonic frequency was given. This frequency is in good agreement with the experimental one (ω_{comp} = 330–360 cm^{-1}; ω_{exp} = 306 cm^{-1}).

3.3.4. $[Cu_3O_2L_3]^{3+6}$

The $[Cu_3O_2L_3]^{3+}$ was recently the subject of serious experimental [63,64] and theoretical investigation [64–66]. This system, shown in Fig. 21 is indeed extremely interesting since it is the first 3:1 metal:O_2 complex which shows oxygen scission (d(O–O) = 2.37 Å).

In fact, contrary to what happen in nature, where each of the copper atom in the Cu active sites supplies only one electron to reduce O_2, here one of the copper atoms supplies two electrons and the other two 1 electron each thus leading to a formal Cu(II)–Cu(II)–Cu(III)–O_2^{2-} complex.

All experimental data (NMR, SQUID, MCD [63,64]) are consistent with a description of a polynuclear complex built up from two paramagnetic $S = 1/2$ Cu(II) centres, ferromagnetically coupled to give an $S = 1$ ground state and one diamagnetic (d^8) Cu(III). The system is experimentally characterised as a completely localised mixed valence system where a hole is localised on the d^8 Cu(III) center.

Previous studies [64] based on a model system where each of the ligands (L = *N*-Permethylated (1*R*,2*R*)-cyclohexanediamine) was substituted by two ammonia molecules, showed that the localisation is driven by the Jahn–Teller effect [67].

In fact, the computed electronic structure for the S = 1 state in the highest symmetry possible for the model compound (i.e. D_{3h}) shows that the SOMOs are of a_2'' and e_1'' symmetry. The resulting degenerate $^3E'$ ground state is, therefore, subject to Jahn–Teller instability and it will distort to remove the degeneracy. The distortion mode (Q_{JT}) can be derived by a symmetry argument and it leads to a descent in symmetry from D_{3h} to C_{2v}.

By performing a set of structural optimisations on the model systems both in D_{3h} and in C_{2v} we determined the minimum energy localised structure and the values of

[6] L = *N*-Permethylated (1*R*,2*R*)-cyclohexanediamine

Table 5
Jahn–Teller parameters computed [a] for the model system $[Cu_3O_2(NH_3)_6]^{3+}$

	LDA	BP	PW91	LDA_{rel}	BP_{rel}	$PW91_{rel}$
E_{JT}	0.192	0.185	0.183	0.203	0.188	0.190
Δ	9.54	−8.01	3.84	11.00	−3.94	5.16
R_{JT}	1.93	0.13	0.15	0.11	0.30	0.12

E_{JT} in eV, Δ in cm^{-1} and R_{JT} in Å [68]. Rel, Pauli relativistic.
[a] Calculations performed using the ADF2000.02 QM/MM implementation [70]. Orbitals up to 3p for Cu, and 1s for N and O were kept frozen; valence shell of H, N, O were described by a double-ζ STO set plus one polarisation function. In the case of Cu atoms a valence triple-ζ plus one polarisation function STO basis was used.

the Jahn Teller parameters (Δ, R_{JT} and E_{JT}) reported in Table 5

Using the methodology of Daul et al. [69] the full potential energy surface corresponding to the $E\text{–}e$ Jahn–Teller coupling was also computed.

Concerning the calculation of the isotropic coupling constant (J^{ex}), Root et al. [64] computed the J value using the BS approach obtaining a value of 878 cm^{-1} which greatly overestimates the experimental value (14 cm^{-1} [64]). They attribute the large difference between the experimental and the theoretical value to the fact that in the BS approach the contribution of the close lying LUMO is neglected. We applied the SD method and computed the full spin manifold arising from the occupation of the SOMO ($12b_2$ and $9a_2$) and of the LUMO ($13b_2$): a two electrons in three orbital problem. Thus we obtain one SD for $(12b_2)^2$, one SD for $(9a_2)^2$, one SD for $(13b_2)^2$, four SD for $(9a_2)^1(12b_2)^1$, four SD for $(9a_2)^1(13b_2)^1$ and four SD for $(12b_2)^1(13b_2)^1$, i.e. a total of fifteen microstates. Out of this set, the energy of only nine of them (the so-called non redundant SDs) is needed. They are represented in Fig. 22 below.

By computing the energy $E(i)$ of the nine NRSD depicted in Fig. 22 above, we can get the energies of the nine spin states (four $^1A_1$, two $^1B_1$, two $^3B_1$ and one $^3A_1$) via the following relationships:

$$^1A_1 = \begin{bmatrix} E(4) & -E(0)+E(7) & -E(5)+E(6) & 0 \\ -E(0)+E(7) & E(1) & -E(8)+E(3) & 0 \\ -E(5)+E(6) & -E(8)+E(3) & E(2) & 0 \\ 0 & 0 & 0 & -E(8)+2E(3) \end{bmatrix}$$

$$^1B_1 = \begin{bmatrix} -E(0)+E(7) & 0 \\ 0 & -E(5)+2E(6) \end{bmatrix}$$

Table 6
Computed energy of the different spin states (at the LDA and GGA level) of the $[Cu_3O_2(NH_3)_6]^{3+}$ model system

	LDA_{rel}	$PW91_{rel}$	BP_{rel}
1^3B_1	0	0	0
2^3B_1	0.4974	0.5148	0.5293
1^3A_1	0.3348	0.9848	0.3629
1^1A_1	0.2015	0.3710	0.1026
2^1A_1	0.8803	0.8509	0.8853
3^1A_1	0.5960	2.5405	1.9353
4^1A_1	2.7188	2.7046	2.9830
1^1B_1	0.6696	0.4559	0.4634
2^1B_1	0.8807	0.8077	0.8131

Energy in eV.

$$^3B_1 = \begin{bmatrix} E(0) & 0 \\ 0 & E(5) \end{bmatrix}$$

$$^3A_1 = E(8)$$

The resulting spin state energies are collected in Table 6 with respect to the energy of the $^3B_1$ ground state.

It is easy to notice that the results we obtain are not better than those of Cole et al. Therefore the large error in the triplet singlet energy gap can not be ascribed fully to the methodology used.

To understand the effect of the structural model on the computed spin manifold we performed two different types of calculation. First we simply used the crystallographic position of the $Cu_3O_2N_6$ core and saturate the N with three H and compute at this frozen geometry the triplet–singlet gap. Next we considered the full system and included the ligand at a QM level and fully optimised the structure using a QM/MM approach. In particular we included in the QM core the $Cu_3O_2N_6$ where the link bonds have been capped by hydrogen atoms while the ligand part was modeled at the MM level using the AMBER force field. The QM core was treated at a GGA BP level. The resulting structure shows a core topology similar to that of the model system except for one structural parameter the NCuN angle. This angle is dramatically reduced (about 10°) leading to better agreement with the experimental values. On this optimised structure we computed the spin manifold at the full QM level using the SD method (always using the BP exchange-correlation functional). The results obtained for the triplet–singlet energy gap are reported in Table 7.

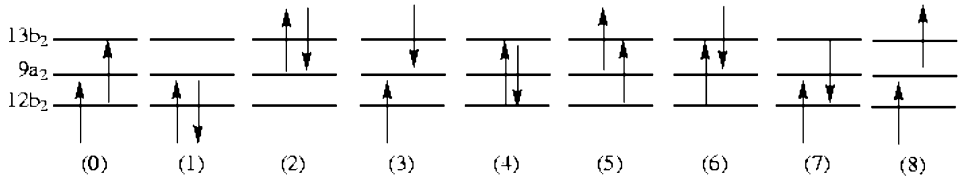

Fig. 22. Schematic representation of the nine non-redundant single determinants (NRSD).

Table 7
Computed triplet–singlet energy gap for $[Cu_3O_2L_3]^{3+}$ and related models

	$\Delta(T-S)$
$[Cu_3O_2(NH_3)_6]^{3+}$ [a]	827
$[Cu_3O_2(NH_3)_6]^{3+}$ [b]	25/550
$[Cu_3O_2L_3]^{3+}$ [c]	72
$[Cu_3O_2L_3]^{3+}$ [d]	157/340
Experimental	14

[a] Optimised model geometry; BP_{rel} level.
[b] Xray $[Cu_3O_2N_6]$ core structure; BP_{rel}. The two values correspond to the two different crystallographic units.
[c] Optimised real system geometry at QM/MM level; BP level.
[d] X-ray $[Cu_3O_2L_3]^{3+}$ structure BP level. The two values correspond to the two different crystallographic units.

From all these results, the following conclusions can be drawn:

- neglecting the full ligand mainly has structural effects (i.e. the change of the NCuN angle) which indirectly affects the computed spin manifold;
- the direct effect of the ligand on the electronic structure of the core is negligible since the results obtained for a model of the X-ray structure (25 and 550 cm^{-1}) and the full X-ray structure (157 and 340 cm^{-1}) are practically equivalent within the error range of the methodology;
- the model retains all the electronic features of the system in terms of exchange and super-exchange pathways but allows for a structural flexibility that the real system does not posses.

We conclude that the model we used influences only the triplet singlet energy gap due to structural effects while from an electronic point of view it correctly reproduces the core of the system. It also worthwhile to recall that discrepancies between the experimental and the computed values are also due to the approximations implicit in the methodology we apply and better agreement is not expected if not fortuitous.

Finally, we can conclude that when dealing with complex molecular system, a QM/MM approach for structural optimisation combined with a DFT calculations for the spin manifold do yield a quantitative description of the magnetic properties of the system.

4. Concluding remarks

We have given in this work a short overview of the calculation of molecular magnetic properties using DFT. A comparison between the DFT based approach and post HF ones was reported in the case of small model systems. From our and other results available in the literature, we can conclude that the prediction of molecular magnetic properties with chemical accuracy is still a difficult task for DFT. The problem we have to face is the accurate calculation of multiplet structure with very small splitting. Hence, the problem reduces to the proper treatment of near degeneracy correlation. We believe that progress in this field will depend upon the development in the future of new functionals, which will include this interaction in some way. Probably, many-body wave-function theory will be needed for this purpose. In this respect, we point out Density Matrix Renormalisation Groups [71] applied to quantum chemistry might play a key role in the near future.

Nevertheless, we have shown in this review that the prediction of magnetic exchange coupling constants: J_{ex} is feasible for fairly large systems, provided that $|J_{ex}|$ exceeds 100 cm^{-1}, i.e. for large and moderately large coupling. Moreover, we have shown that DFT applied to molecular magnetism does accurately describe magneto-structural correlation and yields an illuminating insight into the exchange pathways involved.

Acknowledgements

This work is supported by the Swiss National Science Foundation and by the Swiss Federal Office for Education and Science.

References

[1] (a) R. Caballol, O. Castell, F. Illas, I. Moreira, P.R. de Malrieu, J. Phys. Chem. A 101 (1997) 7860;
(b) A. Ceulemans, G.A. Heylen, L.F. Chibotaru, T.L. Maes, K. Pierloot, C. Ribbing, L.G. Vanquickenborne, Inorg. Chim. Acta 251 (1996) 15;
(c) M.M. Turnbull, T. Sugimoto, L.K. Thompson, (eds.) Molecule-Based Magnetic Materials: Theory, Techniques, and Applications: ACS Symposium Series 644, Washington, DC, 1966.
[2] (a) K. Awaga, T. Sugano, M. Kinoshita, Solid State Commun. 57 (1986) 453;
(b) K. Awaga, Y. Maruyama, J. Chem. Phys. 91 (1989) 2743;
(c) J. Veciana, C. Rovira, O. Armet, V.M. Domingo, M.I. Crespo, F. Palacio, J. Am. Chem. Soc. 113 (1991) 2552;
(d) A. Rajca, S. Utamapayana, J. Am. Chem. Soc. 115 (1993) 2396.
[3] (a) C. Benelli, A. Caneschi, D. Gatteschi, L. Pardi, in: D. Gatteschi, O. Kahn, J.S. Miller, F. Palacio (Eds.), Magnetic Molecular Material, Kluwer, Dordrecht, The Neatherlands, 1991, p. 233;
(b) A. Caneschi, D. Gatteschi, P. Rey, Prog. Inorg. Chem. 39 (1991) 331;
(c) A. Dei, D. Gatteschi, Inorg. Chim. Acta 1992, 813.
[4] (a) K. Sauer, Acc. Chem. Res. 13 (1980) 249;
(b) T.G. Spiro (Ed.), Iron–Sulfur Proteins, Wiley, New York, 1982;
(c) Iron–sulfur proteins, R. Cammack, (ed.), Adv. Inorg. Chem., vol. 38; Academic Press, Inc; San Diego, 1992.;
(d) J. Barber, Nature 376 (1995) 388;
(e) R.H. Holm, P. Kennepohl, E.I. Solomon, Chem. Rev. 96 (1996) 2239.

[5] J.H. Van Vleck, The Theory of Electric and Magnetic Susceptibilities, Oxford University Press, Oxford, 1932.
[6] C.J. O'Connor, Prog. Inorg. Chem. 29 (1982) 203.
[7] I. Dzyaloshinsky, J. Phys. Chem. Solids 4 (1958) 241.
[8] J.H. Van Vleck, J. Phys. Radium 12 (1951) 262.
[9] P.W. Anderson, H. Hasegawa, Phys. Rev. 100 (1955) 675.
[10] C. Zener, Phys. Rev. 81 (1951) 440.
[11] J.J. Borras, E. Coronado, B.S. Tsukerblat, R. Georges, Molecular Magnetism: From Molecular assemblies to the Devices, Kluwer Academic Publisher, Dordrecht, 1996.
[12] P.J. Hay, J.C. Thibeault, R. Hoffman, J. Am. Chem. Soc. 97 (1975) 4884.
[13] B. Briat, O. Kahn, J. Chem. Soc. Faraday II 72 (1976) 268.
[14] P.W. Anderson, Theory of magnetic exchange interactions: exchange in insulators and semiconductors, in: G.T. Rado, H. Suhl (Eds.), Magnetism, vol. 1, Acc. Press, 1963.
[15] (a) J.B. Goodenough, Phys. Rev. 100 (1955) 564;
(b) J.B. Goodenough, Phys. Chem. Solids 6 (1958) 287;
(c) J. Kanamori, Phys. Chem. Solids 10 (1959) 87.
[16] (a) B.C. Guha, Proc. Roy. Soc. (London) Ser A 1951, 353.;
(b) H.U. Gudel, A. Stebler, A. Furrer, Inorg. Chem. 18 (1979) 1021.
[17] P. De Loth, P. Cassoux, J.P. Daudey, J.P. Malrieu, J. Am. Chem. Soc. 103 (1981) 4007.
[18] (a) L. Noodleman, J.G. Norman, J. Chem. Phys. 70 (1979) 4903;
(b) L. Noodleman, J. Chem. Phys. 74 (1981) 5737;
(c) J.G. Norman, P.B. Ryan, L. Noodleman, J. Am. Chem. Soc. 102 (1980) 4279.
[19] (a) L. Noodleman, D.A. Case, Adv. Inorg. Chem. 38 (1992) 423;
(b) L. Noodleman, E.R. Davidson, Chem. Phys. 109 (1986) 131;
(c) J.M. Mouesca, L. Noodleman, D.A. Case, B. Lamotte, Inorg. Chem. 34 (1995) 4347.
[20] E. Ruiz, P. Alemany, S. Alvarez, J. Cano, J. Am. Chem. Soc. 119 (1997) 1297.
[21] R. Caballol, O. Castell, F. Illas, I. Moreira, P.R. de, J.P. Malrieu, J. Chem. Phys. A 101 (1997) 7860.
[22] J.-M. Mouesca, J. Chem. Phys. 113 (2000) 10505.
[23] C.A. Daul, Int. J. Quant. Chem. 52 (1994) 867.
[24] C.A. Daul, K. Doclo, A.C. Stükl, in: P.C. Delano (Ed.), Recent Advance in Density Functional Methods, Part II, World Scientific Publisher, 1997, p. 61.
[25] A.A. Ovchinnikov, J.K. Labanowski, Phys. Rev. A 53 (1996) 3946.
[26] J.C. Slater, Quantum Theory of Molecules and Solids. Self-Consistent Field for Molecules and Solids, vol. 4, McGraw-Hill, New York, 1974.
[27] S.H. Vosko, L. Wilk, M. Nusair, Can. J. Phys. 58 (1980) 1200.
[28] H. Stoll, C.M.E. Pavlidou, H. Preuss, Theor. Chim. Acta 49 (1978) 143.
[29] A.D. Becke, Phys. Rev. A 38 (1988) 3098.
[30] J.P. Perdew, Phys. Rev. B 33 (1986) 8822.
[31] C. Lee, W. Yang, R.G. Parr, Phys. Rev. B 37 (1988) 785.
[32] (a) J.P. Perdew, Y. Wang, Phys. Rev. B 33 (1986) 8800;
(b) J.P. Perdew, J.A. Chevary, S.H. Vosko, K.A. Jackson, M.R. Pederson, D.J. Singh, Phys. Rev. A 46 (1992) 6671.
[33] A.D. Becke, J. Chem. Phys. 98 (1993) 5648.
[34] M.J. Frish, G.W. Trucks, H.B. Schlegel, P.M.W. Gill, B.G. Johnson, M.A. Robb, J.R. Cheeseman, T.A. Keith, G.A. Petersson, J.A. Montgomery, K. Rsghavachari, M.A. Al-Laham, V.G. Zakrewski, J.V. Ortiz, J.B. Foresman, J. Cioslowski, B.B. Stefanov, A. Nanayakkara, M. Challacombe, C.Y. Peng, P.Y. Ayala, W. Chen, M.W. Wong, J.L. Andres, E.S. Replogle, R. Gomperts, R.L. Martin, D.J. Fox, J.S. Binkley, D.J. DeFrees, J. Baker, J.P. Stewart, M. Head-Gordon, C. Gonzales, J.A. Pople, GAUSSIAN 94; Gaussian Inc., Pittsburgh, PA, 1996.
[35] Amsterdam Density Functional (ADF) Rev. 2.01–2.3; Vrije Universiteit: Amsterdam 1995.
[36] A. Bencini, F. Totti, C.A. Daul, K. Doclo, V. Barone, Inorg. Chem. 36 (1997) 5022.
[37] M.W. Schmidt, K.K. Baldridge, J.A. Boatz, S.T. Elbert, M.S. Gordon, J.H. Jensen, S. Koseki, N. Matsunaga, K.A. Nguyen, S.J. Su, T.L. Windus, M. Dupuis, J.A. Montgomery, J. Comput. Chem. 14 (1993) 1347.
[38] J.P. Daudey, J.P. Malrieu, D. Maynan, M. Pellisier, F. Spiegelman, R. Caballol, S. Evangelisti, F Illas, J. Rubio, PSHF-CIPSI Program Package.
[39] J.R. Hart, A.K. Rappé, S.M. Gorun, T.H. Upton, J. Phys. Chem. 96 (1992) 6264.
[40] (a) S.C. Abraham, H.J. Williams, J. Phys. Chem. 39 (1963) 2963;
(b) P.H. Vesses, D.R. Fitzwater, R.E. Rundle, Acta Crystallogr. 16 (1963) 1045;
(c) G. Maass, B. Gerstein, R.D. Willett, J. Phys. Chem. 46 (1967) 401.
[41] (a) C. Chow, R.D. Willett, J. Phys. Chem. 59 (1973) 5903;
(b) R.D. Willett, C. Chow, Acta Cristallogr. Sect. B B30 (1974) 207;
(c) A. Bencini, D. Gatteschi, C. Zanchini, Inorg. Chem. 24 (1985) 704.
[42] (a) J. Miralles, J.P. Daudey, R. Caballol, Chem.Phys. Lett. 198 (1992) 555;
(b) J. Miralles, O. Castell, R. Caballol, J.P. Malrieu, Chem. Phys. 172 (1993) 33;
(c) O. Castell, R. Caballol, J. Miralles, Chem.Phys. 179 (1994) 377.
[43] A. Bencini, D. Gatteschi, J. Am. Chem. Soc. 108 (1986) 5763.
[44] C. Adamo, V. Barone, A. Bencini, I. Totti, I. Ciofini, Inorg. Chem. 38 (1999) 1996.
[45] S. Bruni, A. Caneschi, F. Cariati, C. Delfs, A. Dei, D. Gatteschi, J. Am. Chem. Soc. 116 (1994) 1388.
[46] A. Bencini, I. Ciofini, E. Giannasi, C.A. Daul, K. Doclo, Inorg. Chem. 37 (1998) 3719.
[47] Y. Pontillon, A. Bencini, A. Caneschi, A. Dei, D. Gatteschi, B. Gillon, C. Sangregorio, J. Stride, F. Totti, Angew. Chem. Int. Ed. 39 (2000) 1786.
[48] (a) K. Mukai, Bull. Chem. Soc. Jpn. 42 (1969) 40;
(b) M. Kinoshita, Mol. Cryst. Liquid Cryst. 176 (1989) 163.
[49] T. Nogami, K. Tomioka, T. Ishida, H. Yoshikawa, M. Yasui, F. Iwasaki, H. Iwamura, N. Takeda, M. Ishikawa, Chem. Lett. (1994) 29.
[50] (a) K. Awaga, T. Inabe, T. Nakamura, M. Matsumoto, Y. Maruyama, Mol. Cryst. Liquid Cryst. A 232 (1993) 69;
(b) K. Awaga, T. Inabe, T. Nakamura, M. Matsumoto, Y. Maruyama, Sinth. Metals 56 (1993) 3311.
[51] R. Chiarelli, M.A. Novak, A. Rassat, J.L. Tholence, Nature 363 (1993) 147.
[52] V. Barone, A. Bencini, A. di Matteo, J. Am. Chem. Soc. 119 (1997) 10831.
[53] (a) R. Kuhn, H. Trischmann, Angew. Chem. 75 (1963) 294;
(b) R. Kuhn, H. Trischmann, Monatsh. Chem. 95 (1964) 457.
[54] D.J. Brook, H.H. Fox, V. Lynch, M.A. Fox, J. Phys. Chem. 100 (1996) 2066.
[55] V. Barone, A. Bencini, I. Ciofini, C.A. Daul, J. Chem. Phys. A 103 (1999) 4275.
[56] (a) CossiM., V. Barone, R. Cammi, Tomasi, J. Chem. Phys. Lett. 235 (1996) 327;
(b) V. Barone, M. Cossi, N. Rega, J. Chem. Phys. 105 (1996) 11060.
[57] (a) S. Drueke, P. Chaudhuri, K. Pohl, K. Wieghardt, X.Q. Ding, E. Bill, A. Sawaryn, A.X. Trautwein, H. Winkler, S.J. Gurman, J. Chem. Soc. Chem. Commun. (1989) 59.;
(b) DingX.Q., E.L. Bominaar, E. Bill, H. Winkler, A.X. Trautwein, S. Drueke, P. Chaudhuri, Wieghardt, J. Chem. Phys. 92 (1990) 178;

(c) G. Peng, J. Van Elp, H. Jang, L. Que, W.H. Armstrong, S.P. Cramer, J. Am. Chem. Soc. 117 (1995) 2515.
[58] D.R. Gamelin, E.L. Bominaar, M.L. Kirk, K. Wieghardt, E.I. Solomon, J. Am. Chem. Soc. 118 (1996) 8085.
[59] M.B. Robin, P. Day, Adv. Inorg. Chem. Radiochem. 10 (1967) 247.
[60] L. Noodleman, E. Baerends, J. Am. Chem. Soc. 106 (1984) 2316.
[61] V. Barone, A. Bencini, I. Ciofini, F. Totti, C.A. Daul, J. Am. Chem. Soc. 128 (1998) 8357.
[62] G. Blondin, J.-J. Girerd, Chem. Rev. 90 (1990) 1359.
[63] A.P. Cole, D.E. Root, P. Mukherjee, E.I. Solomon, T.D.P. Stack, Science 273 (1996) 1848.
[64] D.E. Root, M.J. Henson, T. Machonkin, P. Mukherjee, T.D.P. Stack, E.I. Solomon, J. Am. Chem. Soc. 120 (1998) 4982.
[65] A. Bérces, Chem. Eur. J. 4 (1998) 1297.
[66] C.A. Daul, S. Fernandez-Ceballos, I. Ciofini, C. Rauzy, C.-W. Schlaepfer, Chem. A. Eur. J. 8 (2002) 4392.
[67] H.A. Jahn, E. Teller, Proc. R. Soc. A 161 (1937) 220.
[68] E. Gamp, Doctoral Thesis.
[69] (a) T.K. Kundu, R. Bruyndonckx, C.A. Daul, P.T. Manoharan, Inorg. Chem. 38 (1999) 3931;
(b) R. Bruyndonckx, C. Daul, P.T. Manoharan, E. Deiss, Inorg. Chem. 36 (1997) 4251.
[70] (a) T.K. Woo, L. Cavallo, T. Ziegler, Theor. Chem. Acc 100 (1998) 307;
(b) F. Maseras, K. Morokuma, J. Comp. Chem. 16 (1995) 1170.
[71] S.R. White, R.L. Martin, J. Chem. Phys. 110 (1999) 4127.